Effects of naval traffic on sediment erosion and accumulation in ports: a new model-based methodology

Antonio Guarnieri [(1)], Sina Saremi [(2)], Andrea Pedroncini[(3)] Jacob H. Jensen[(2)], Silvia Torretta[(3)] Marco Vaccari[(4)], Caterina Vincenzi [(4)]

(1) Istituto Nazionale di Geofisica e Vulcanologia, Sezione di Bologna, Via D. Creti, 12, 40128 Bologna, Italy

(2) DHI, Horsholm, Denmark

(3) DHI S.r.l., Via Bombrini 11/12, 16149 Genova

(4) Autorità di Sistema Portuale del Mar Ligure Occidentale (Genova), Palazzo San Giorgio - Via della Mercanzia 2

Corresponding author: Antonio Guarnieri; antonio.guarnieri@ingv.it

Abstract

The action of propeller-induced jets on the seabed of ports can cause erosion and the deposition of sediment around the port basin, potentially significantly impacting on the bottom topography over the medium and long time. If such dynamics are constantly repeated for long periods, a drastic reduction in ships' clearance can result through accretion, or it can threaten the stability and duration of structures through erosion. These sediment-related processes present port managing authorities with problems, both in terms of navigation safety and in the optimization of management and maintenance activities of the ports' bottom and infrastructures.

In this study, which is based on integrated numerical modeling, we examine the hydrodynamics and the related bottom sediment erosion and accumulation patterns induced by the action of vessel propellers in the passenger port of Genoa (Italy). The proposed new methodology offers a state-of-the-art science-based tool that can be used to optimize and efficiently plan port management and seabed maintenance.

1 - Introduction

The operational activities of harbors and ports are closely related to the local bathymetry, which must be sufficiently deep to guarantee the regular passage, maneuvering and berthing of ships. However, ship clearance is often so limited that it threatens the safety of in-port navigation, and ships may even hit the seabed in extreme cases. This is therefore a source of criticalities that often result in management and maintenance efficiency problems in terms of the bottom and a port's infrastructure in general (Mujal-Colilles et al., 2016; Castells-Sanabra et al., 2020).

The action of a ship's main propellers means that traffic in ports is responsible for generating intense current jets, as noted in Figure 1. The high velocities induce shear stresses on the sea bottom, which can possibly result in sediment resuspension when they exceed the critical stress point for erosion (Van Rijn, 2007, Soulsby et al., 1993; Grant and Madsen, 1979). Before depositing back onto the sea floor the re-suspended sediment may be transported widely around the basin by the combined effects of natural currents such as those induced by tides, winds or density gradients, and by vessel-related currents, such as those induced by the propellers or the movement and displacement of ships. The continuous traffic in and out ports can thus result in the displacement of a huge volume of seabed material, which can then induce significant variations in the bathymetry over medium to long time scales. The formation of erosional or depositional trends in specific areas of port basins can potentially result from these variations.

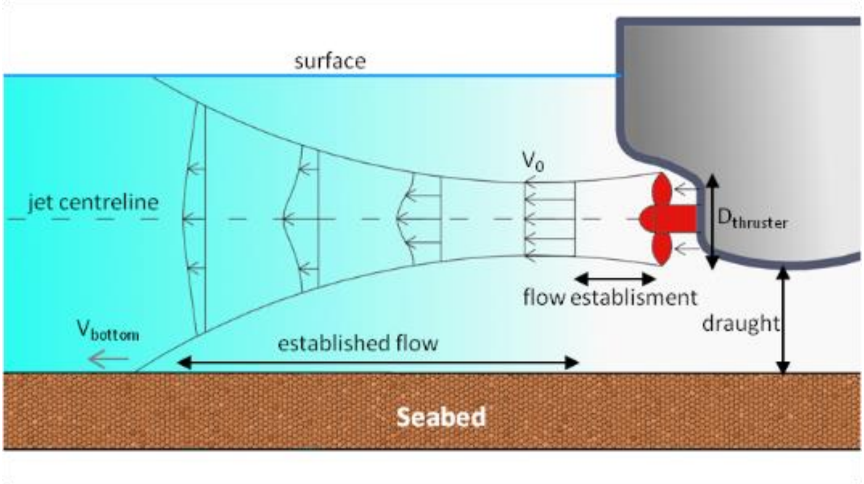

Figure 1 - Example of propeller induced jet of a moving ship (main propulsion without rudder)

If such dynamics are particularly pronounced and rapid (bottom accretion of an order of tens of centimeters per year or even higher), the port authorities must undergo dredging operations for the maintenance of the seabed, to fully recover the clearance and ensure the conditions necessary for undisturbed ships motion, maneuvering and docking/undocking operations.

Most of the published literature about the effects of ships' propellers on port sediments and structures is experimental, and is mainly conducted in laboratories using physical models (Mujal-Colilles et al. 2018; Yuksel et al. 2019). Few practical instruments are available for port authorities that can provide robust and scientifically based analyses and predictions of the relevant processes. Such tools can enable them to plan specific actions aimed at maintaining the seabed, and thus help both guarantee the continuity of operational activities of ports and optimize the use of economic resources. Unplanned maintenance activities usually involve additional costs due to the need to operate in emergency conditions and in some cases partially interrupt the service.

The integrated numerical modeling of hydrodynamics and sediment transport represents an important aid to port authorities, and more broadly to port managers and operators, as suggested by Mujal-Colilles (2018). This can reproduce and thus provide a better understanding of the seabed sediment dynamics induced by ships' propellers over short, medium and long time scales, thus establishing what tools are required to ensure the efficient operational maintenance of the seabed.

Propeller induced jets have mainly been studied using empirical formulas based on specific characteristics of the ships and ports of interest, such as the bathymetry, propeller typology, diameter and rotation rate, and ship's draught. The most common approaches are the German method (MarCorm WG, 2015; Grabe, et al., 2015; Abromeit et al., 2010,) and the Dutch method (CIRIA et al., 2007). The resulting induced velocities are usually only considered locally, to inform the technical design of mooring structures and the protection of a port's infrastructure. Although various assumptions are introduced through empirical formulas, these approaches are limited and do not fully consider the three-dimensional evolution of the induced jet throughout the water column at any distance from the propeller, or at any location of the port. These tools are therefore not suitable for the comprehensive management of ports.

We conduct a pilot study of the hydrodynamics and seabed evolution induced by ships' propellers in the passenger area of the Port of Genoa (Figure 2), where the naval traffic involves mainly passenger vessels (ferries and cruise ships, generally self-propelled) and in which the resulting sediment dynamics in terms of erosion/deposition rates are particularly significant: estimated in the order of several tens of centimeters per year (as directly estimated and communicated by the Port Operators and via an analysis of bathymetric surveys). In this study, we propose that the integrated high-resolution numerical modeling of three-dimensional hydrodynamics and sediment transport can be a robust and science-based tool for the optimization and efficient planning of port management and maintenance activities. We propose a new methodology that can be used in a delayed mode, and can thus reproduce the historical major sediment processes over time, as in this study, or in a prediction mode through the potential implementation of real-time operational services.

The remainder of this paper is organized as follows: in Sect. 2 we introduce our methodology, and the data available for the study are presented in Sect. 3. Sect. 4 describes the numerical models used, and the results of the numerical simulations are presented and discussed in Sect. 5. Finally, the summary and conclusions of the work are given in Sect. 6.

2 – Methods

The study is based on the latest versions of the hydrodynamic and mud transport models MIKE 3 FM (DHI, 2017), which are described in detail in Sect. 3 and in APPENDICES A1 and A2. A very high resolution was used in the numerical model to realistically reproduce the propeller induced jet, both in the vertical and in the horizontal, at approximately 1-2 meters and 5 meters, respectively. Together with a non-hydrostatic version of the hydrodynamic model, this enables the processes and dominant patterns of the current field generated by the ships propellers during the navigation and maneuvering inside the port to be reproduced very accurately.

As shown in Figure 2, 12 docks have been included in the study (marked with orange or red lines indicating ferry or cruise vessels, respectively). The Port Authority mainly focused on passenger vessels as they considered their effect on the seabed to be greater than other types of vessels that have much less frequent passage. Moreover, passenger ships are in general self-propelled, while other vessel types are often driven by tugboats. We therefore only simulated passenger ships.

The turning basins in which arriving vessels undergo maneuvers for berthing are represented in Figure 2 by the white-dashed circles marked *a* and *b*. Circle *a* refers to vessels berthing at docks T5 to T11, while circle *b* refers to vessels for docks T1 to T3. Finally, the turning area for vessels arriving at docks D.L., 1012 and 1003 is at the entrance of the port and is not simulated in this study, as it is out of our area of interest.

The general methodology can be separated into the following phases.

1. *Assessment of the naval traffic during a typical year*. This phase is fundamental, as it identifies the typical dynamics of the naval traffic in the different sectors of the port and the characteristics of the ships that have the greatest effect on the hydrodynamics and sediment re-suspension on the bottom. These include the size of the ships, the related draught, the dimension of the propellers and their typical rotation rates. The results of the analysis, which are discussed in detail in Sect. 4.1, also enabled representative synthetic vessels for each berth of the port to be defined.
2. *Implementation of a high-resolution 3D hydrodynamic model of the port of Genoa*. This numerical hydrodynamic model considered ship routes, both entering and exiting the port, as established through the previous vessel traffic analysis phase. As detailed in Sect. 4.1, 24 simulations of the hydrodynamic model have been implemented, one for each dock and route considered (docking and undocking). The resulting 24 scenarios were then simulated separately. This enabled us to analyze the effect of each vessel's passage on the induced hydrodynamics of the basin. Each hydrodynamic contribution was then used to drive the sediment transport model. This approach does not consider potential simultaneous interactions amongst hydrodynamic patterns generated by different propellers, as we assume that vessels are unlikely to pass each other very closely.
3. *Implementation of a coupled sediment transport model*. Based on the available data, a numerical model of sediment resuspension and transport for fine-grained and cohesive material was then implemented. The model was combined with the hydrodynamics resulting from the 24 different vessels scenarios. The simulations of the sediment model were conducted separately for the hydrodynamic component.

4. *Collating the results and the overall analysis*. The effects of the passage of the single vessels on the bottom sediment were then combined in terms of the erosion/deposition resulting from the overall number of passages over the analyzed one-year period of time. This enabled us to provide aggregated information on the annual sediment dynamics.

We then conducted a semi-quantitative calibration/validation of the modeling results through a comparison of the seabed evolution reproduced using the integrated modeling system and the various bathymetric maps derived from surveys of the port topography at approximately one year intervals.

The proposed approach assumes that each hydrodynamic and sediment transport simulation uses the same bathymetry as the initial bottom condition. Although this assumption may have implications, as we explain in the results section, it does not compromise the main conclusions of the study.

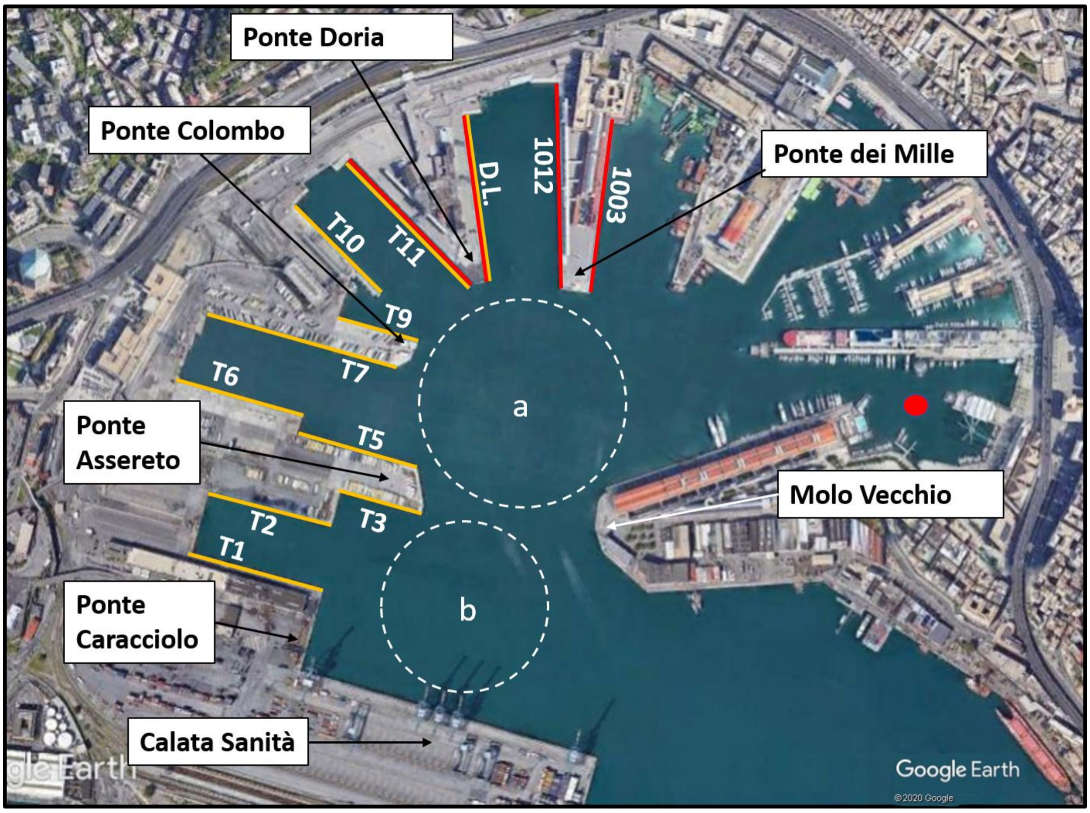

Figure 2 - Passenger port of Genoa. The colored lines along the docks refer to the typology of the operating ships: red lines indicate cruise vessels while orange lines indicate ferries. The names of the docks (in white) are next to the colored lines are. The red dot represents the location of the station where sediment samples with physical information on the grains are available (see Sect. 4.2). The white dashed circles marked as *a* and *b* represent the turning areas for vessels berthing to docks T5 to T11 and to T1 to T3

3 – Available data and information

Most of the data necessary for this project were provided by the Port Authority of Genoa and Stazioni Marittime SpA, the main port operator in the area.

3.1 – Bathymetry

Several bathymetry surveys of the sectors of the port were available at various resolutions. The dataset used for the simulations was obtained by merging the latest available surveys (March-June 2018) of the inner sectors of the port, delivered on a regular grid of five meters of resolution. Figure 3 shows the merged bathymetry for the entire port (left panel) and for a detail of the Ponte Colombo and the surrounding basin. The main area of interest for the study (from the line between Calatà Sanità and Molo Vecchio to the end of the Port, see Figure 2) measures approximately 0.60 km^2 and has an average depth of approximately 13 meters. The bathymetry is in general heterogeneous. The wet basins are approximately 10-11 meters deep, while areas shallower than 10 meters are present only in the eastern part of the basin, where yachts and non-commercial vessels operate. A deep natural pit is clearly visible a few tens of meters off the right edge of *Ponte Colombo* and *Ponte Assereto*, extending approximately 22 meters below the water surface. The Port Authority has regarded this area as a preferred site for dumping the sediment resulting from regular maintenance dredging operations of the seabed, in sectors where depositional trends are large enough to reduce vessels clearance and to affect the safety of navigation inside the port. This depressed area is also used as a turning area by passenger ferries heading to docks T5, T6, T7 and T9, which cover approximately 50% of the naval traffic in the basin (see Sect. 4.1). During their manoeuvres over this pit the turning ferries produce intense turbulence, which may reach the newly dumped material resulting from the dredging operations. This material is still loose and can consequently be easily re-suspended and transported around the port basin, thus making the dredging operations ineffective.

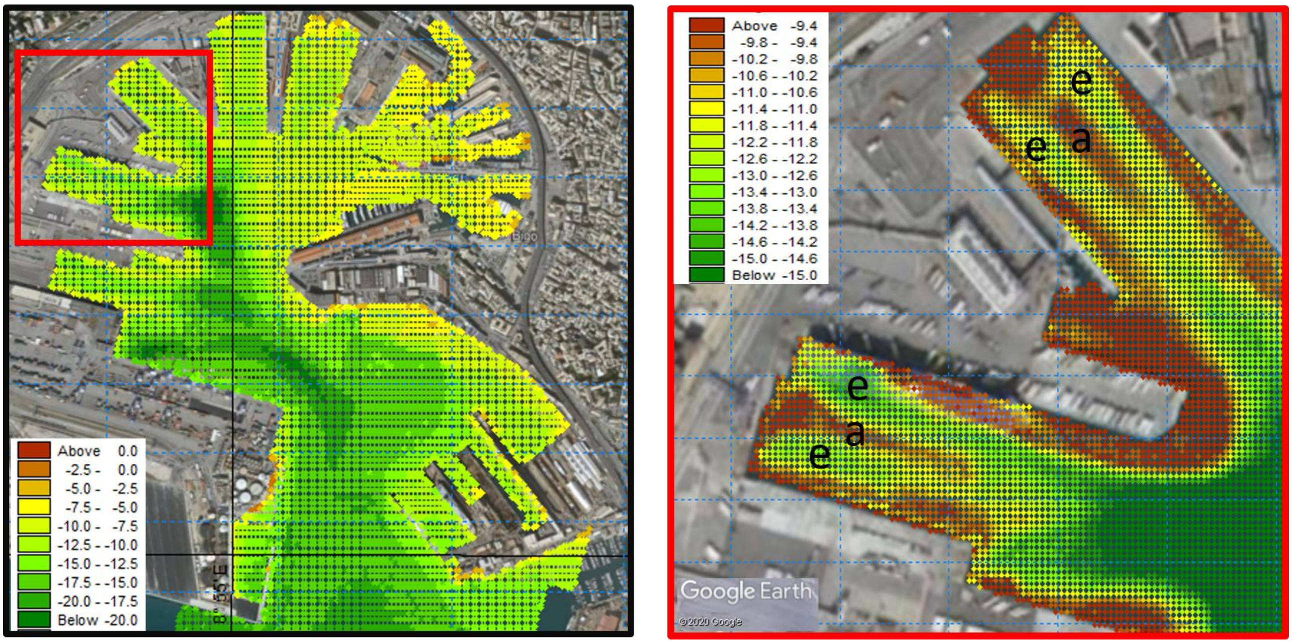

Figure 3 - Bathymetry of the port of Genoa. Entire Passenger Port (left panel) and zoom on *Ponte Colombo* and the surrounding basins (from T5 to T11, right panel)

The bathymetry presented in the right panel of Figure 3 follows the pattern of erosion and accumulation common to wet basins confined among docks. The propeller activity when vessels leave or approach the berth induces areas of erosion, identified by channels of deepened bathymetry (referred to with an "*e*" in the right panel of Figure 3, and coloured yellow-green) and areas of accumulation identified with tongues of shallower bathymetry (denoted by "*a*" in the right panel of Figure 3, and coloured brown).

Another survey covering approximately the same area as that of Figure 3 is available for the period May-June 2017. By comparing the topographical information of the two and integrating the information on dredging activities during the same period, we were able to reconstruct in a semi-quantitative fashion the sediment dynamics occurring during this time window of approximately one year. This information was then used in the calibration/validation process for the numerical model of sediment erosion and transport, as detailed in Sect. 5.

3.2 – Sediment data

The availability of information on sediment textures in the sea is limited. We were able to access the MArine Coastal Information sySTEm (MACISTE; http://www.apge.macisteweb.com) implemented by the Department of Science of Earth, Environment and Life (DISTAV) of the University of Genova, where the results of several chemical and physical sediment surveys are stored and are accessible. Unfortunately, although the chemical information is comprehensive, information on grain size for the inner area of the port is incomplete. The red dot of Figure 2 represents the only location inside the basin where information on the texture composition and grain size was available. These characteristics are necessary for the sediment transport model and in the simulations for the entire domain of the numerical model (see Sect. 4.2).

3.3 – Naval traffic

In terms of naval traffic, 2017 was considered by the Port Authority of Genoa and Stazioni Marittime SpA to be a typical year. The traffic data were available on a daily basis and included information on the docks of arrival/departure and the names of the vessels involved. The entire year was considered, to account for the typical seasonality of the traffic concentration, which is particularly significant for passenger vessels from the end of spring to the beginning of fall.

The characteristics of the vessels required for the modelling activity (i.e. length, width, tonnage, draught) were obtained from information available through public sources. The outcomes of the analysis are presented in Sect. 4.1.

4 – The numerical models

The non-hydrostatic version of the MIKE 3 HD flow model (DHI, 2017) was used to simulate the propeller induced three-dimensional current along the port basin. The resulting hydrodynamic field was coupled with the sediment transport module MIKE 3 MT (DHI, 2019), suitable for fine-grained and cohesive material, in order to drive the erosion, advection-dispersion and deposition of fine sediment along the water column.

4.1 – The hydrodynamic model

The MIKE 3 FM flow model is an ocean circulation model suitable for different applications within oceanographic, coastal and estuarine environments at global, regional and coastal scales. It is based on the numerical solution of the Navier-Stokes equations for an incompressible fluid in the three dimensions (momentum and continuity equations), based on the advection-diffusion of potential temperature and salinity and on the pressure equation, which in the present non-hydrostatic version is split into hydrostatic and non-hydrostatic components. The closure of the model is obtained by the choice of a turbulence closure formulation with various possible options within a constant value, and a logarithmic law scheme or a k-ε scheme, which is used in the present implementation. The surface is free to move and it can be solved using a sigma coordinate (as used in the present study) or a combined sigma-zed approach. The spatial discretization of the governing equations of the model follows a cell-centred finite volume method. In our implementation of the model we used the barotropic density mode, and thus temperature, salinity and consequently density were constant in time and space during the simulations.

The domain of the present implementation of the model is presented in the upper panels of Figure 4. The images show two examples of computational grids used for the simulations. Here, the docks are T1 (left panel) and T10 (right panel) during inbound operations. The grids are a combination of unstructured triangular and quadrilateral cells with horizontal resolutions varying from 30 meters in the furthest areas from the ship trajectory to 5 meters approximately within the closest area to the ships' propellers. The mesh is rectangular in areas where the ships are moving straight ahead and the 5 meter resolution covers a corridor of approximately 50 meters of width. In the manoeuvring areas, the mesh becomes unstructured and the resolution is again 5 meters. The red lines in the middle of the five-meter resolution corridors of the upper panels represent the routes followed by the ships inside the port. The lower panels of the figure are snapshots taken from the web service https://www.marinetraffic.com, which show the actual routes of the vessels birthing in the docks in the upper panels (T1 and T10) as recorded by the AIS system mounted on the ships. As shown in Figure 4 the reconstructed trajectories of the ships in the model are realistic and fully representative of the real trajectories.

Table 1 shows the results of the traffic analysis within the Port of Genoa for 2017 conducted using the daily traffic data provided by Stazioni Marittime SpA. The annual traffic is generally regular, and its frequency varies from basin to basin and depends on the season. Generally, the busiest docks are T5, T6 and T7, accounting for almost 50% of the total traffic. They follow an approximately daily frequency all year round, whereas the wet basins towards the end of the port, which mainly serve cruise vessels, show an evident seasonality, probably related to the Mediterranean cruise season (few and irregular passages from January to May, then regular and in a much increased frequency from June to October/November).

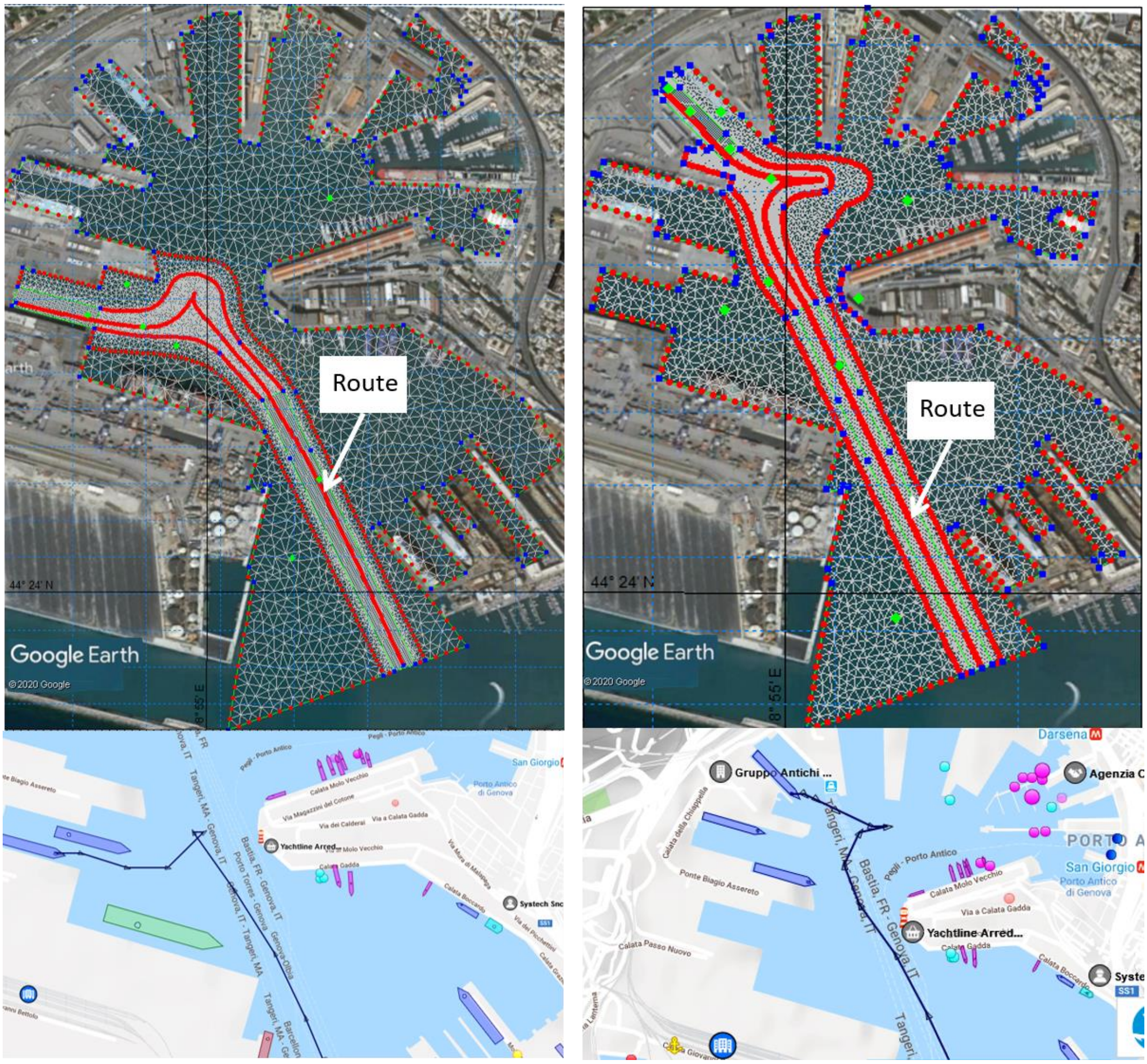

Figure 4 - Model domain and computational grids for docking routes of T1 (left panel) and T10 (right panel) docks. In the lower panels the corresponding actual routes are shown

Table 1 - Analysis of ship traffic in the port of Genoa for year 2017 and main characteristics of the ship representative of each dock. The ship's length, width, draught and propeller's diameter values are expressed in meters

Dock	**Number of Berthing**	**% Berthing**	**Average Length [m]**	**Average Width [m]**	**Average Draught [m]**	**Average Diameter [m]**
1012	122	6.4%	318.41	37.86	8.33	5.80
1003	47	2.5%	276.20	30.07	7.45	5.20
D.L.	12	0.6%	290.86	32.02	7.82	5.40
T11	123	6.4%	213.23	31.67	7.16	5.20
T10	202	10.5%	181.88	26.44	6.46	4.70
T9	8	0.4%	152.96	24.81	5.91	4.40
T7	308	16.1%	214.27	26.45	6.85	4.90

T6	291	15.2%	204.93	26.35	6.62	4.80
T5	351	18.3%	203.93	29.57	6.95	5.00
T3	87	4.5%	155.16	25.60	6.17	4.50
T2	202	10.5%	185.66	27.85	6.68	4.80
T1	164	8.6%	204.00	28.33	6.93	5.00
TOTALE	**1917**	100.0%	---	---	---	

In the vertical, the model is resolved over 10 evenly distributed sigma layers. The resulting layer depths vary from approximately 1 meter in the berthing areas to approximately 2 meters in the pits and in the areas closer to the port's entrance.

4.1.1 - Propeller jet velocity

The propellers' maximum jet velocity was calculated based on the Code of Practice of the Federal Waterways Engineering and Research Institute (Abromeit et al., 2010) and the PIANC Report n. 180 (MarCom WG 180, 2015), taking the German approach. The relevant parameters for the calculations are shown in Figure 1. The maximum velocity V_0 after the jet contraction generated by the propeller is developed along its axis. For unducted propellers, we use Eq. (1a) for the propeller ratio $J=0$ (ship not moving) or Eq. (1b) for $J\neq 0$ (moving ship).

$$V_0 = 1.60 f_n\, n_d D \sqrt{K_T} \qquad (1a)$$

$$V_{0j} = \frac{\sqrt{(J^2 + 2.55 K_{Tj})}}{\sqrt{1.4\frac{P}{D}}} V_0 \qquad (1b)$$

where n_d [1/s] is the design rotation rate of the propeller; f_n is the factor for the applicable propeller rotation rate (non-dimensional); D is the propeller diameter [m]; K_t or K_{tj} is the thrust coefficient of the propeller (non-dimensional) in the case of non-motion or motion of the ship, respectively; and P is the design pitch [m]. Typical values for fn are 0.7 - 0.8 during manoeuvring activities, while the P/D ratio can be assumed to be approximately equal to 0.7. K_t or K_{tj} can be estimated through Eq. (2a) and (2b), according to the state of motion of the ship:

$$K_t = 0.55\frac{P}{D} \qquad (2a)$$

$$K_{tj} = 0.55\frac{P}{D} - 0.46J \qquad (2b)$$

The propeller ratio J depends on a wake factor w, which varies from 0.20 to 0.45 (non-dimensional), and on the velocity of the ship according to Eq. (3):

$$J = \frac{v_{s(1-w)}}{nD} \qquad (3)$$

As proposed by Hamill (1987) and further described by Lam et al. (2005), the downstream propeller-induced jet is divided into a zone of flow establishment (closer to the propeller) and a zone of established flow (further downstream). The resulting velocity V_0 used in the model to calculate the corresponding discharge and momentum sources is considered as the maximum velocity at the beginning of the zone of the established flow.

As we had no direct information about the size of the ship's propellers, we referred to the specific literature. For the propellers of the Ro-Ro ferries that typically serve docks T1, T2, T3, T5, T6, T7, T9, T10 and T11, we referred to the report n° 02 of the project "Mitigating and reversing the side-effects of environmental legislation on Ro-Ro shipping in Northern Europe" (Kristensen, 2016) implemented by the Technical University of Denmark (DTU) and HOK Marineconsult ApS. According to this study, the relationship between the draught and the diameter of the ferry's propeller is given by Eq. (4):

$$D_{prop} = 0.56 \times H_{draught} + 1.07 \quad (4)$$

where D_{prop} is the propeller's diameter [m], and $H_{draught}$ is the maximum draft of the ship [m]. This relation is not valid for cruise ships, as they typically have larger propellers. For this type of ship, which serve docks 1012, 1002 and partially D.L. and T11, we directly referenced operators in the passenger ship design sector, and double checked the information with the formulas from Eq. (4) and from Eq. (5), which is also valid for double propeller passenger ships. This qualitative analysis provided the diameters presented in Table 1.

$$D_{prop} = 0.85 \times H_{draft} - 0.69 \quad (5)$$

The water discharge was obtained by combining the diameter of the propeller and the intensity of the jet, which was discretized into a certain number of smaller discharges associated with various smaller sources of momentum in the numerical model. We thus realistically represented the propeller. The distribution of volume and momentum sources follows a spatially Gaussian (normal) distribution with a discretization step of 0.5 meters and a constant rotation rate of the propeller.

Figure 5 shows the propeller's induced jet in the hydrodynamic model. The left panel represents the plan of Dock 1012, where a large cruise ship is departing. The solid line of the upper left panel is the location of the vertical transect shown in the upper right image, representing the jet velocity in the plane *xz*. The dashed line in the upper left panel represents the trajectory followed by the axis of the departing ship, and the associated jet's velocity in the *yz* plane is shown in the bottom panel. Although the horizontal resolution is non-optimal in terms of propeller representation, the resulting jet appears extremely realistic both in transverse and longitudinal directions.

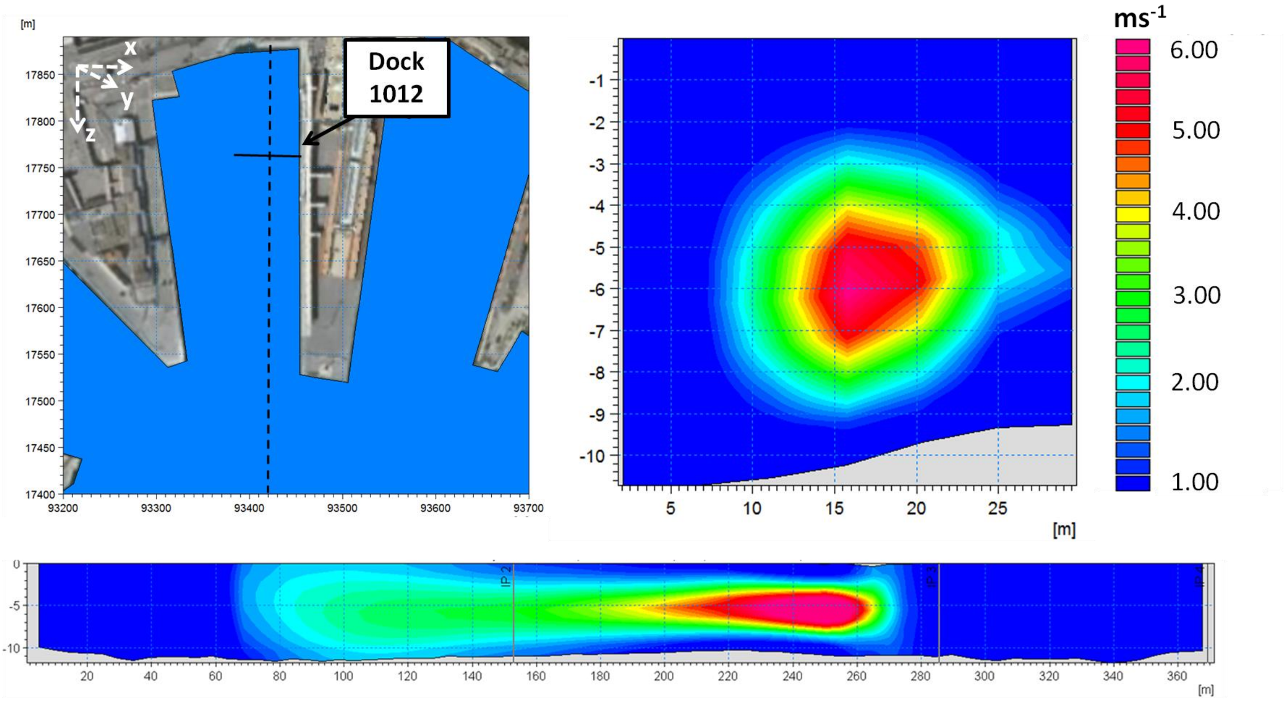

Figure 5 – Representation of the propeller-induced jet of the most representative ship departing from Dock 1012. Left: plan view; the dashed line represents the trajectory followed by the axis of the undocking ship, the solid line represents the position of the vertical transect shown in the upper right panel, showing the jet's induced velocity in the *xz* plane (propeller's plane). Lower panel: transect of velocity along the propellers axis (*yz* plane). Velocities are in ms^{-1}

To preserve the water mass budget, we associated a sink to each source. Sinks are prescribed in terms of negative equivalent discharge (m^3s^{-1}) in the grid cell adjacent to that hosting the source, in the direction of the ship motion (sinks precede corresponding sources).

The choice of the vertical and horizontal resolutions of the hydrodynamic model were the result of a thorough sensitivity analysis of the grid's cell dimensions. We assumed that the most appropriate resolution for the model allows the maximum (jet centreline) current produced by the combined discharge and momentum sources in the model to reach the input maximum velocity of V_0. For the sensitivity analysis, we considered a 4-meter diameter propeller with a rotation rate of two rounds per second (rps) at full power. According to Eq. (1b), this configuration results in a V_0 of approximately 6 ms^{-1} at the depth of the propeller's axis once the jet is fully developed. We set up an experimental configuration domain 100 meters wide and 500 meters long. We tested horizontal resolutions of 20 m, 10 m, 5 m, 2 m and 1 m, while for the vertical we considered two configurations: 10 and 20 layers in a constant bathymetry of 20 meters. The input value of the jet current to the model was 6 ms^{-1}.

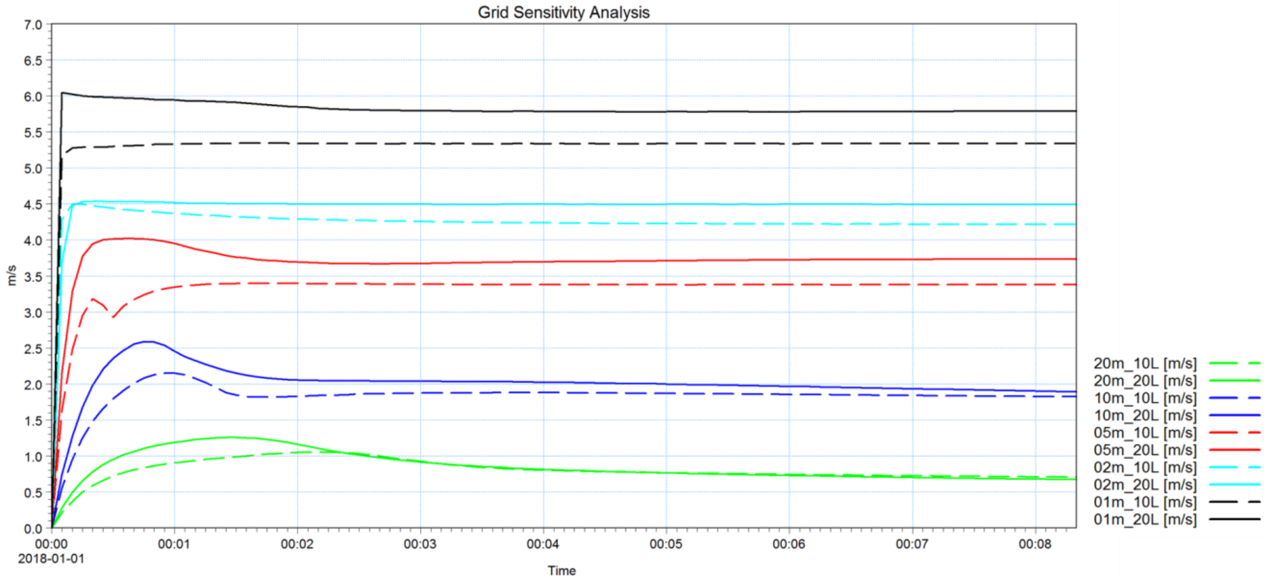

Figure 6 – Model grid sensitivity analysis to the cells dimension. The different colors correspond to the different horizontal resolution. Dashed lines indicate the configurations with 10 layers while solid lines indicate those with 20 layers

Figure 6 shows the sensitivity analysis of the grid resolution. The resulting velocity at the propeller's axis is proportional to the resolution, both in the vertical and the horizontal: the higher the resolution, the higher the resulting velocity. The most appropriate grid is that with a 1-meter resolution and 20 vertical layers, which is the only configuration of the model that allows the jet to reach the maximum speed imposed as the input. However, this configuration would require approximately 1 year of computational time to run the 24 simulations implemented in this study in the same computational configurations, which is obviously unrealistic. We thus sought a compromise between acceptable computational demand and realistic resulting velocity. The final configuration took 5 meters as the horizontal resolution and 10 vertical levels. As these resolutions did not allow for the complete development of the current speed, we introduced a correction to the input velocity of each simulated vessel by increasing it by the necessary amount to reach the empirically calculated V_{0}. This involved considerable additional time for manual calibration.

4.1.2 – Forcing and boundary conditions

Due to the nature of the focal processes, we only account for the force of the propellers of the vessels. The jet induced by its motion is of an order of magnitude of several meters per second in the area surrounding the blades and when unconstrained it has a length of influence of at least 40-50 times the propeller's diameter behind the ship (Verhei, 1983). This is also an important source of toe scouring in the presence of a quay wall (Hamill & Johnston 1999). Natural forcing such as wind, density gradients or tides are one to two orders of magnitude smaller, and can thus be neglected without introducing errors that can potentially affect sediment resuspension from the bottom. However, the Bernoulli wake may be responsible for currents of comparable intensity (Rapaglia et al., 2011), although smaller, and can be a forcing source in the system. Anyhow, we do not consider this due to technical complications and time constraints. Including such a process in further developments and analysing its impact on the overall dynamics of ship-induced sediment transport would be of interest. Our final results prove satisfactory, suggesting that the governing processes for these dynamics are associated more with propeller-induced currents than with the motion of the ship itself, likely due to the limited speeds of vessels in this inner part of the harbour and to the relatively large volume of water available for each passing vessel.

The boundaries of the hydrodynamic domain are the docks around the basin and the port entrance, which is the only open boundary. Here we imposed a Flather condition (1976) assuming constant zero velocities and levels. This allowed us to minimize the boundary effects, albeit with some interference between the flux and the boundary line (not shown). However, due to the distance between the open boundary line and the berthing areas, such effects do not influence the results of the study. A zero normal velocity was imposed along the closed boundaries.

4.2 – The sediment transport model

The hydrodynamic model was coupled with a sediment transport model – MIKE 3 MT FM - valid for fine-grained and cohesive sediment (diameter smaller than 63 µm, Lisi et al., 2017). This is the main type of sediment in the port of Genoa and is particularly relevant in terms of erosion, transport and further deposition, as its small particle dimension and light weight rapidly lead to its resuspension and advection around the basin.

The equations of the mud transport model are based on the advection and dispersion (AD) of the sediment concentration along the water column and are detailed in APPENDIX A2. The AD equation is solved using an explicit, third order finite difference scheme called ULTIMATE (Leonard, 1991).

The model consists of two areas: a water and a seabed environment. The seabed is represented through a multi-bed layer and multi-fraction approach in which the layers can exchange mass and only the top level is active, thus making it available for erosion. The different layers are defined by the proportions of sediment in their composition, the degree of consolidation of the sediment within each layer, and the thickness of the single layer. The sediment proportions are described through their associated physical characteristics, and are eroded and deposited proportionally to their concentration both in the bed texture and along the water column. Flocculation processes occur in the water environment of the model when a certain concentration threshold is exceeded (here assumed to be equal to 0.01 gl^{-1}), while at a threshold of 10 gl^{-1} settling is hindered, according to the definition of Winterwerp and Kesteren (2004). The deposition of the sediment is based on a Teeter (1986) profile and the threshold for deposition used was 0.07 Nm^{-2}. The sediment grain diameter is defined through the associated settling velocity, based on Stokes' law. In the interface between the water and the bottom the sediment may be eroded, as proposed by Partheniades (1965) for consolidated sediment or by Parchure and Metha (1985) for soft or unconsolidated sediment. In both cases the sediment is eroded and injected into the water column when the shear stress resulting from the current, the wave action or a combination of both exceeds a certain critical value. We do not consider waves as our focus is inside the port.

The specific equations and parameterizations referred to in the sediment model are summarized in APPENDIX A2.

4.2.1 - Sediment characteristics

Three sediment surveys were conducted between June 2009 and July 2010. Table 2 presents the results of the surveys in terms of percentage and class of sediment per survey (last and central column, respectively). Given the nature of our study, our focus is on mud and fine sand, and thus grains coarser than 2 mm were not considered.

Table 2 - Sediment size data inside the port (see station identified with the red dot of Figure 2). Three different surveys were carried out between June 2009 and July 2010

Date of survey	Sediment Size	%
2009-06-15 16:00:00	Ø < 63 µm	82.4
2009-06-15 16:00:00	63µm < Ø < 2mm	16.2
2009-06-15 16:00:00	Ø > 2 mm	1.4
2009-07-15 16:00:00	Ø < 63 µm	89.2
2009-07-15 16:00:00	63µm < Ø < 2mm	9.1
2009-07-15 16:00:00	Ø > 2 mm	1.7
2010-07-28 09:00:00	Ø < 63 µm	78.2
2010-07-28 09:00:00	63µm < Ø < 2mm	17.7

We assumed that the proportions of the samples with Ø < 63 µm were composed of two grain sizes with diameters of 30 μm and 50 μm, respectively, while for the observed components with diameters in the range of 63μm to 2 mm we assumed 100 μm to be representative.

The degree of consolidation of the seabed is both time- and depth-dependent. The upper layer, which mostly contributes to the flux of re-suspended sediments into the water column, is composed of freshly deposited sediment as it is subject to continuous reworking. The lower layers are more consolidated, and the degree of consolidation increases by depth. This vertical gradient in seabed properties is enhanced in a port environment as the upper layers are continuously influenced by the propeller induced jets several times per day, hence a multilayer modelling of the seabed is appropriate. Teisson (1993) and Sandford and Maa (2001) also took this approach. A single layer bed representation would imply an overestimation of the bed's erodibility (soft mud, thus easily reworked), resulting in unrealistic further overestimations of sediment erosion and concentration along the water column. Thus, a multilayer representation of the seabed is required to account for the transition from unconsolidated to consolidated material. Amorim et al. (2010) used a two-layer approach to model the seabed with MIKE software, simulating the sediment transport in the navigation channel of the Port of Santos. However, as they suggested, a two-layer representation of the seabed may produce an unrealistically abrupt transition between erodible and hard bed layers, so to consider a gradual transition from freshly deposited to consolidated material, three bed layers were defined here, representing the freshly deposited, slightly consolidated and fully consolidated sediments. The percentage of the fine particles in the sediment texture was assumed to decrease proportionally to the depth of the layers. Thus, the first layer contained 80% of fine grains (50% of grains of Ø=30 μm and 30% of Ø=50 μm) and 20% of coarse (Ø=100μm), while the third layer contained 50% of coarse (Ø=100μm) and 50% of fine (20% of grains of Ø=30 μm and 30% of Ø=50 μm). In the mid layer, an even distribution was assumed among the three. The thicknesses of the three layers are 0.5 *mm*, 1 *mm* and 50 *mm* at the beginning of each scenario. The first layer is composed of very soft mud as it is the result of the newly deposited and finer mud. The other two layers are more consolidated and thicker, as they are less easily eroded and are shielded by the upper layers. The different layers and fractions of sediment that characterise the bottom enabled us to represent the port bed in a complex and comprehensive way, and include the various degrees of consolidation of the layers and the resulting responses to shear stress.

The main characteristics of the layers and sediment proportions implemented in the sediment transport model are presented in Table 3.

Finally, sediment input may also potentially come from six minor streams that flow into the port area. These have very modest basins of approximately 1 km^2 on average, and have been ceiling-covered for many years, so they now act more as sewage collectors than natural streams. Their contribution to the sedimentary dynamics of the port of Genoa has been estimated and the annual sediment supply to the port basin from each stream evaluated, based on the method proposed by Ciccacci et al. (1989). The estimated sediment contribution was only a few hundreds of cubic meters per year in the worst case, which corresponds to a contribution to the wet basins of a few millimetres of annual accumulated sediment from the surrounding river inlet. This level of solid matter has not been considered in the model as the erosional and depositional processes induced by the propeller activity are higher by one or two orders of magnitude.

Table 3 – Summary of sediment characteristics as implemented in the mud transport model

Parameter	**Layer 1**	**Layer 2**	**Layer 3**
Layer thickness (mm)	0.5	1	50
Type of Mud	Soft	hard	hard
Dry density of bed layer (kgm^{-3})	180	300	450
Parameter	**Fraction 1**	**Fraction 2**	**Fraction 3**
Φ (µm)	30	50	100
% of fraction in layer 1, 2, 3	50, 33, 20	30, 33, 30	20, 33, 50
W_s (mms^{-1})	0.7	2.2	8.8
τ_{ce} (Pa)	0.15	0.25	0.5
τ_{cd} (Pa)	0.07	0.07	0.07
C_{floc} (gl^{-1})	0.01	0.01	0.01
C_{hind} (gl^{-1})	10	10	10

ρ_s (kgm^{-3})	2650	2650	2650

5 — Results and discussion

The main results of the hydrodynamic and sediment transport model are presented in this section. Due to the large number of simulations carried out, only those regarding two docks are shown. However, the current and sediment concentration results corresponding to the other simulations are qualitatively similar. We focus on the simulations of docks 1012 and T7. Dock 1012 is particularly important as it hosts the largest passenger vessels operating in the port, while dock T7 has a high frequency of passages.

Figure 7 shows the propeller-generated current in the bottom layer and at the depth of the propeller's axis (upper right and left panels, respectively) and the resulting suspended sediment concentration in the same layers (corresponding lower panels) during the departure of a cruise vessel from dock 1012. The characteristics of a vessel representative of the traffic in the dock are given in Table 1. When departing, the engine operates close to full power, which we assume results in a rotation rate of two rounds per second (rps) for the propeller. This induces a maximum velocity at the depth of the propeller axis close to 9 ms^{-1}, which is damped to approximately 2 ms^{-1} on the bottom of the berthing basin along the vessel's route. This intense jet is deflected to the left due to the head wall of the berthing basin, which constrains the flow and induces a cyclonic eddy that is well developed along the whole water column. The cone-like envelope of the jet in the vertical plane, as illustrated in the theoretical scheme of Figure 1 can be observed in the upper panels of Figure 7, which refer to the same example: the influence of the propeller on the bottom occurs several tens of meters behind the propeller's position, and the velocity at the bottom is much reduced. The induced eddy in the wet basin acts as a trap for the eroded sediment, which enters the cyclonic gyre (or anti-cyclonic in the case of departure from the opposite dock) and tends to deposit in the middle of the basin, where the fluxes progressively decrease. The position of the eye of the cyclone evolves parallel to the docks' longitudinal walls and induces the sediment trapped inside the gyre to sink along the longitudinal axis of the wet basin. Such dynamic occurs similarly for all the horseshoe-shaped wet basins, inducing accumulation along the central portions. The re-suspended sediment may reach very high concentrations of up to several hundreds of mgl^{-1} in the bottom layers, depending on the different specific characteristics of the sediment texture (such as grain size, level of consolidation and availability to erosion) and of the vessel (such as dimensions of the propellers, rotation rate and draught).

Various hydro and sediment dynamics occur during the inbound phase of vessels manoeuvring inside the port. Most of the manoeuvring operations (i.e. when vessels rotate within a turning basin and proceed backwards to the docks) occur in the turning basins denoted by the dashed circles *a* and *b* in Figure 2. The engines operate at high power when starting the manoeuvre, to allow for the rotation of the ship. The vessel's longitudinal axis then rapidly changes direction (from tens of seconds up to a few minutes) and can span wide angles, depending on the specific manoeuvre. The propeller induced jet follows the same rotation along the horizontal plane, resulting in a fan-like distributed set of directions for the associated currents. Such operations are realistically represented by the model, as shown in Figure 8, which refers to the berthing of the vessel representative of dock T7. The currents shown in the figure are those associated with the propeller's axis during four different moments of the turning manoeuvre. Each panel refers to successive time intervals of approximately 100 seconds. These successive instants are presented in the order of up-left, up-right, down-left and down-right. In the lower-right panel the propeller has already changed rotation direction and the vessel is now proceeding backwards. The induced current jet is thus heading towards the centre of the port and pushing the sediment towards this area. The simultaneous seabed activity is shown in Figure 9. Although the jet induced currents are very much weaker at the seabed than those at the depth of the propeller's axis, they are still significant and may reach intensities of up to 1 ms^{-1}, depending on the local bathymetry.

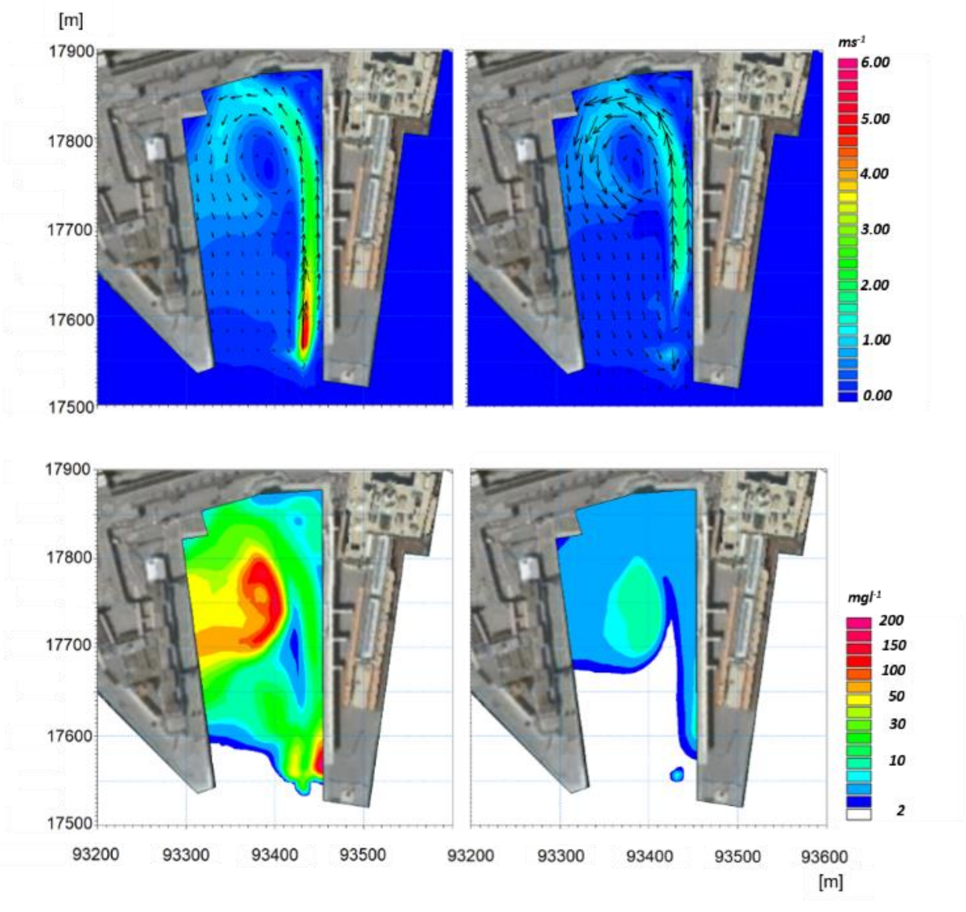

Figure 7 – Results of the numerical models. Upper panels: current intensity and direction in the bottom layer (right) and in the layer corresponding to the axis propeller. Lower panels: resulting suspended sediment

concentration (SSC, mgl^{-1}) in the same layers as the upper panels. The images refer to the undocking of the cruise vessel representative of dock 1012.

The current distribution at the seabed is much more chaotic than at the propeller's axis depth. This area of the port corresponds to the natural pit (which reaches approximately 22 meters below the surface in the deeper part) in which the material dredged from the accumulation areas is often dumped during the sea bottom maintenance activities. The dashed line shown in the lower-right panels of Figure 8 and Figure 9 refers to the transect presented in Figure 10, in the same instant (i.e. when the vessel has ended the manoeuvre in the circle *b* and is approaching dock T7 backwards).

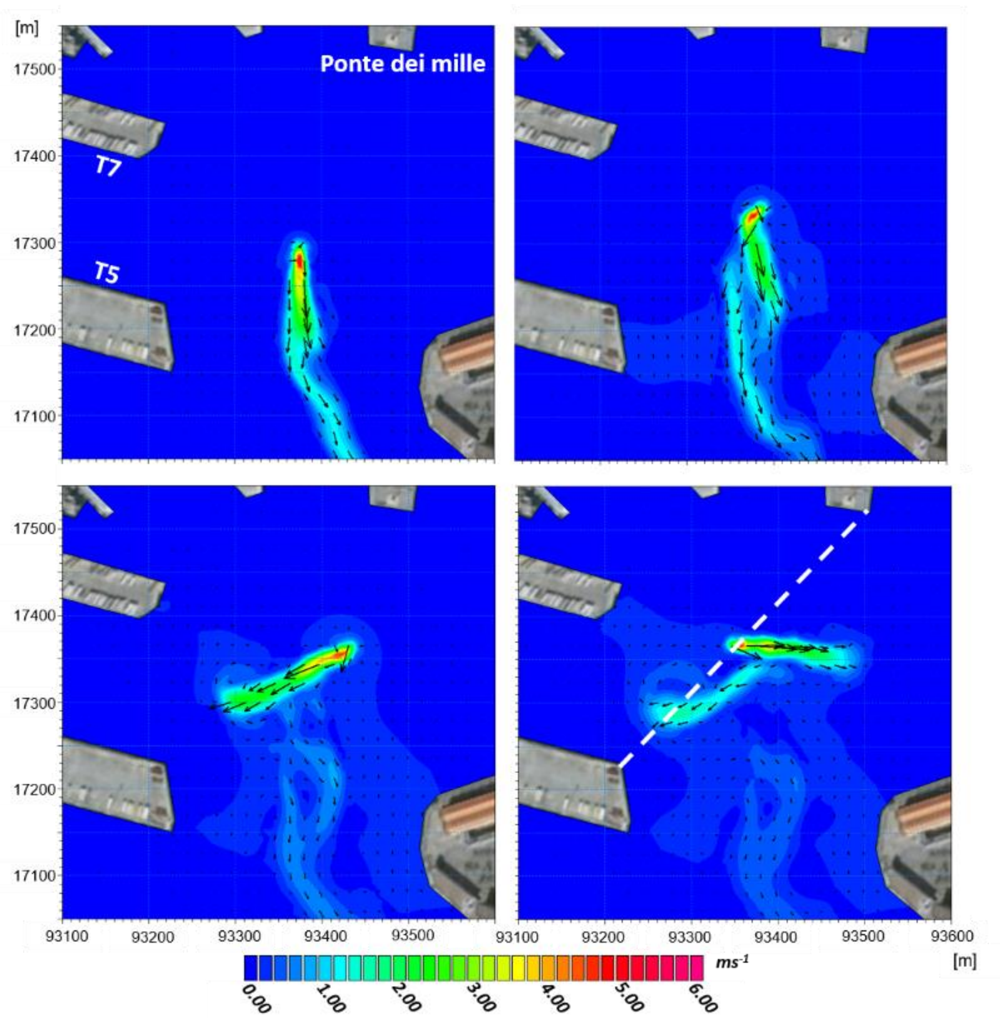

Figure 8 – Results of the hydrodynamic model at the depth of the propeller's axis. Each panel refers to a time interval of approximately 100 seconds from the previous one. The temporal order of the panels is up-left, up-right, down-left and down-right. The images refer to docking maneuvers of the Ro-Ro vessel representative of dock T7

A combined analysis of Figure 8, Figure 9, and Figure 10 helps us understand the dynamics occurring in the turning basin *b* during the manoeuvres when approaching docks T5, T6 and T7, and particularly the overall sediment dynamics of the entire port, as these three docks account for approximately half of the entire passenger traffic. The propeller-induced velocities at the bottom of the natural pit during turning manoeuvres are variable and may exceed 1 ms^{-1}, which is a significant current intensity that can entrain and move a large amount of sediment. The resulting re-suspended sediment concentration may reach values exceeding 50-60 mgl^{-1}, as shown in the lower panel of Figure 10. Once re-suspended from the pit, the sediment is advected by the jet-induced complex field of currents of Figure 8 and Figure 9. This area is typically refilled with freshly dredged material resulting from the seabed maintenance activities, and thus the propeller's induced currents on the bottom have an enhanced erosion effect on the unconsolidated material and can rapidly nullify the benefit of the dredging operations. Thus, the results of the simulations suggest avoiding the use of the natural pit as a dumping area for the resulting material, and confirm that integrated modelling can be an effective tool for simulating the processes and mechanisms related to sediment transport, and for the optimized planning of maintenance activities.

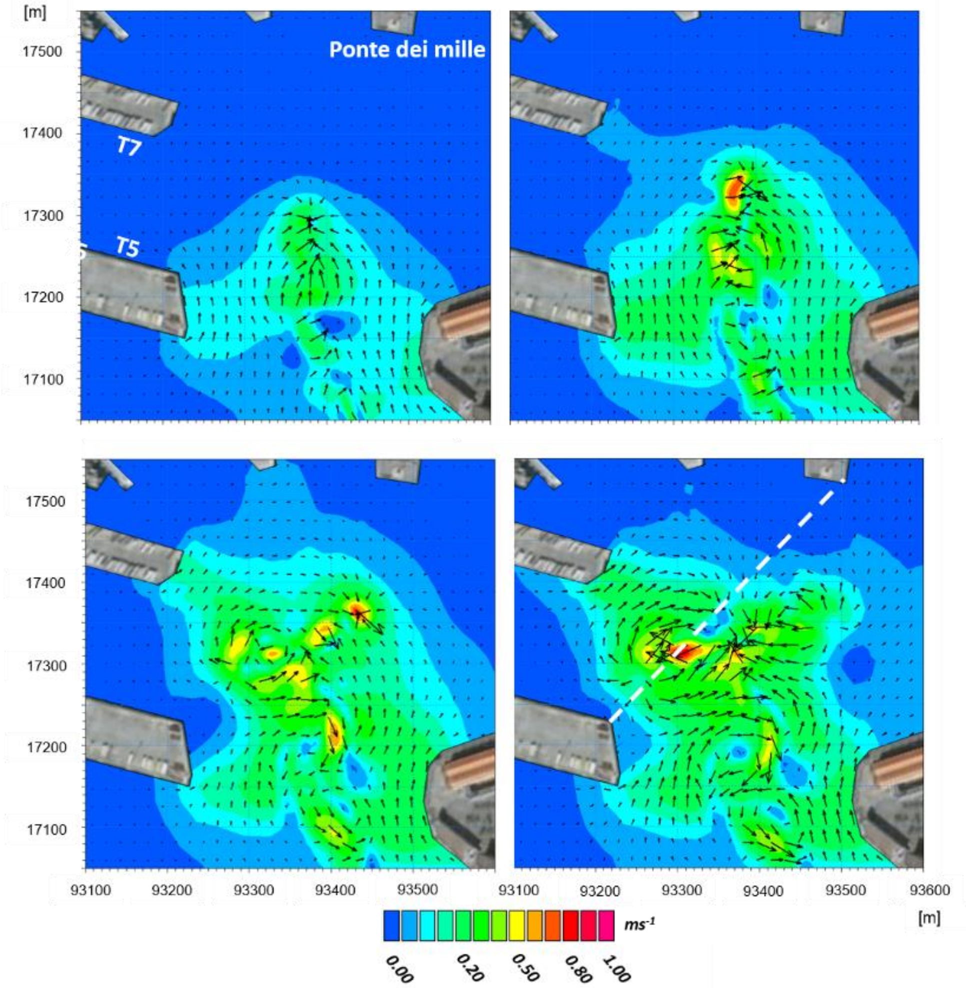

Figure 9 – Results of the hydrodynamic model in the bottom layer. Each panel refers to a time interval of approximately 100 seconds from the previous one. The temporal order of the panels is up-left, up-right, down-left and down-right. The images refer to docking maneuvers of the Ro-Ro vessel representative of dock T7

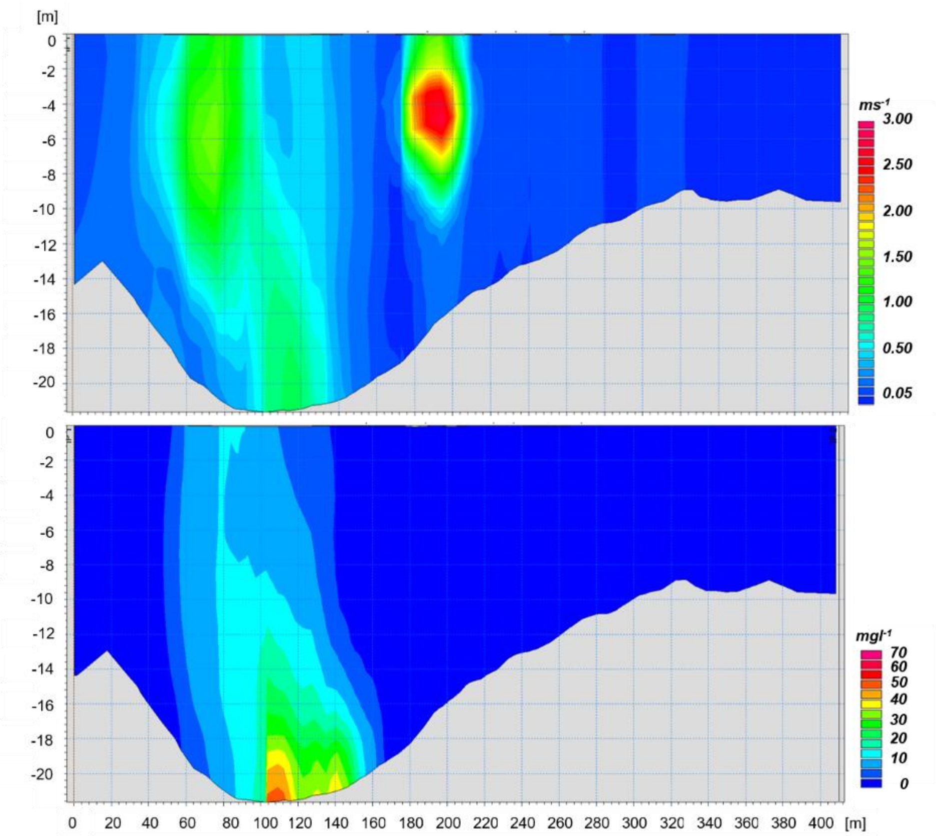

Figure 10 - Velocity intensity in ms^{-1} (upper panel) and sediment concentration in mgl^{-1} (lower panel) along the transect from the head of *Ponte Assereto* to the head of *Ponte dei Mille*

The impact on the bed thickness of the naval traffic is illustrated in Figure 11, which presents the erosion and deposition maps resulting from the simulations of one departure (left) and one arrival (right) of the representative passenger vessels of docks 1012 (up) and T7 (down). The blue color represents areas of erosion, while the red represents the accumulation of the sediment after an interval of time long enough for the re-suspended sediment to completely settle. The left panels of the figure show that during the vessel's departure a considerable amount of material tends to be eroded from the bases of the docks and settles in the center of the mooring basins. This mechanism is clearly related to the vessel's departure (left panels) rather than its arrival (right panels). The erosion underneath the vessel's keel along the ship's trajectory is evident, both during departure and arrival, thus supporting previous experimental findings (Castells et al., 2018). The order of magnitude of erosion and deposition of a single vessel's passage is of a few millimeters in the areas most influenced by the vessel's activity.

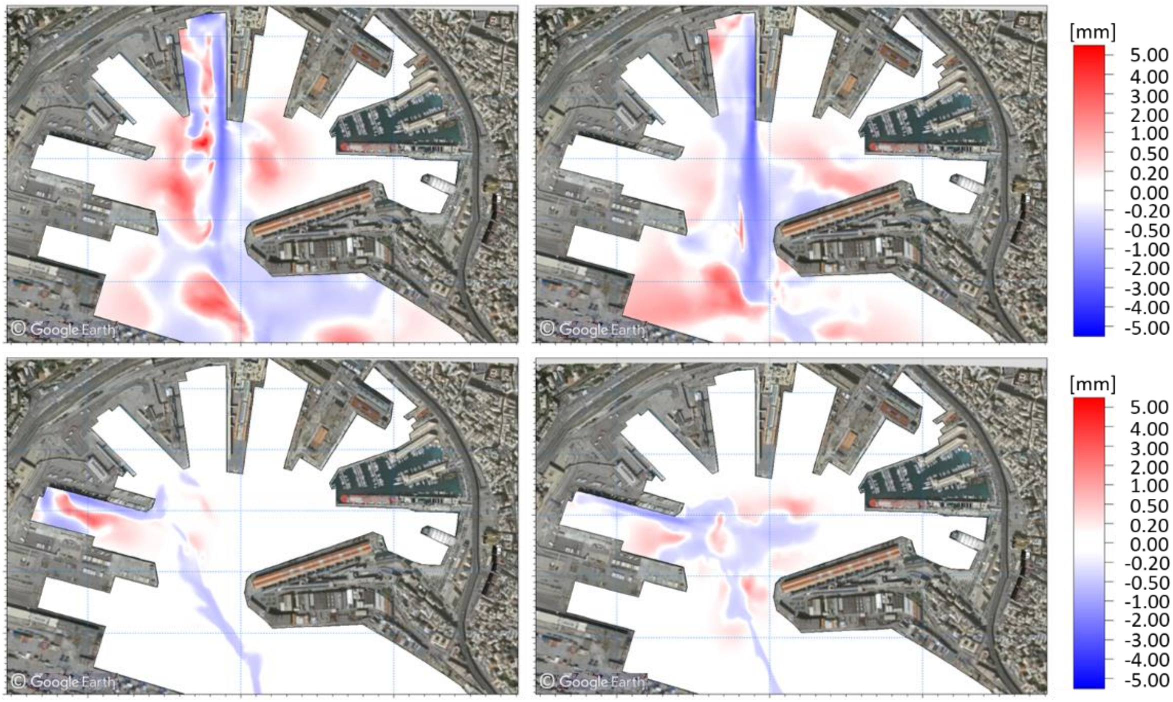

Figure 11 – Erosion and deposition maps resulting from one departure (left) and one arrival (right) of the representative passenger vessels of docks 1012 (up) and T7 (down)

Such impact can become a real threat to the continuity of operations in large and busy ports such as Genoa over medium to long timescales. The few millimeters of accumulation and erosion can become several tens of centimeters after a few thousand annual passages. For the sake of completeness, the results of the impact on the bed thickness due to the activity of the other vessels not shown here are presented in APPENDIX A3.

Based on the traffic analysis of Table 1 we projected each single naval passage to a one-year duration and superimposed the effects of erosion and deposition of vessels that are representative of all of the passenger docks. We were thus able to reconstruct the annual port seabed evolution for the year of 2017. The effects of the single passages were weighted by the specific occurrences of that year, thus obtaining 24 maps (one for each docking and one for each undocking), and the results were integrated to obtain a final map.

As the trajectories for reaching a dock (or departing from it) vary slightly from passage to passage, a Bartlett spatial filter was applied to the integrated results using the values of 4, 2 and 1 as weights. Figure 12 presents the results of this analysis. In the left panel the results from the modeling system in terms of annual erosion (blue) and accumulation (red) are shown, while in the right panel the observed seabed evolution is shown. The observed map was reconstructed using the outcomes of two bathymetric surveys carried out in the periods of May-June 2017 and March-June 2018. The difference in the bathymetries of the two surveys resulted in the evolution of the seabed during the approximate one-year period, except for dredging operations. We indicated the areas where the most significant dynamics took place on the maps using numbers.

The area between the heads of *Ponte dei Mille* and of *Molo Vecchio,* identified as 1, was dredged during the period October-December 2017, and approximately 15.000 m^3 of solid material was removed and dumped into the natural pit of the port, as indicated by the number 5. Thus, what appears to be at first sight an area of erosion due to vessel traffic - area 1 in the right panel of Figure 12 - is actually an area of accumulation, which is confirmed by the fact that dredging operations were conducted. Similarly, the accumulation observed in area 5 (right panel of Figure 12) is not the result of the induced action of the propellers, but of the accumulation of the sediment dumped after the maintenance dredging operations. The model results are in total agreement with these dynamics. As discussed above, the material re-suspended during vessels' maneuvers is likely pushed towards area 1 during the phase of the backward advancing of the vessels when approaching the docks. Conversely, area 5 is partially an area of erosion, as evidenced by the model. The freshly deposited material during dredging operations is thus rapidly re-suspended.

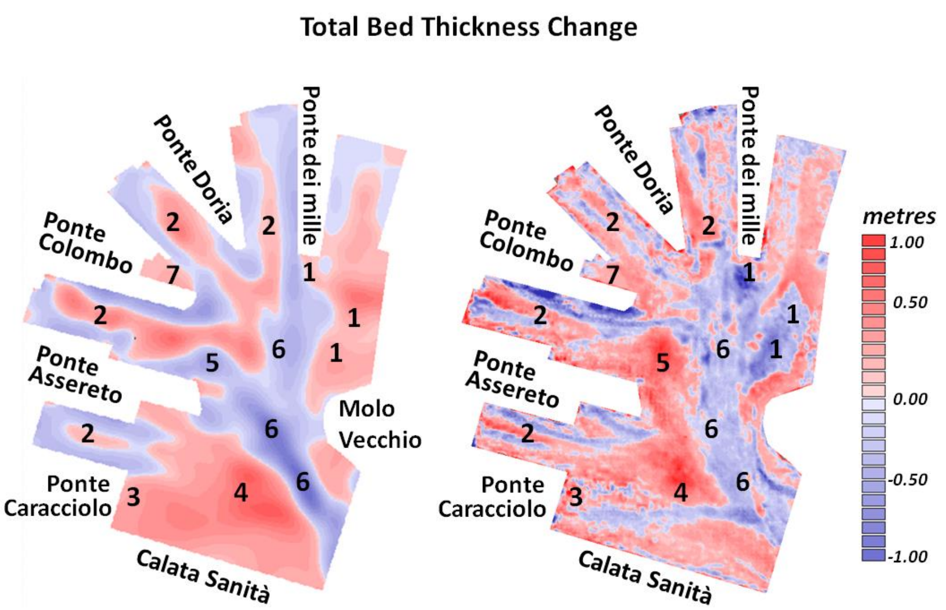

Figure 12 – Annual erosion and deposition map reconstructed on the basis of the hydrodynamic and sediment transport simulations for the year 2017

Area 1 accounts for approximately 30-40 cm of accumulated material per year, with local maxima of up to 50 cm. Similar values were estimated through years of managing experience by the personnel of Stazioni Marittime S.p.A (personal communication).

The central portions of the wet basins marked with number 2 in Figure 12 are areas of deposition, mainly due to the phase of departure of the ships. Again, the model can well reproduce both the accumulation along the central parts of the basins, where it may reach 20 cm per year or even more, and the erosion along the walls of the docks. Here, the propellers' erosive action may result in stability problems for the docks, particularly along the walls of dock 1012, where the biggest cruise vessels operate.

The erosion underneath the vessels' typical routes (i.e. from the entrance to approximately the center of the port) is also well represented by the model, and is identified in the figure with the number 6. The model and the observations also exhibit good agreement in the deposition area (number 7), where a local gyre forms and entraps the suspended sediment. Finally, areas 3 and 4 are also subject to deposition, and qualitative agreement between the model and the various bathymetric surveys is evident from Figure 12. The erosive print observed in the survey under these areas is most likely due to activities related to cargo vessels approaching and departing from dock *Calata Sanità*. These vessels were not the focus of our study, and *Calata Sanità* only operates container ships, and thus the model does not include the naval traffic here.

In general, the observed and the modeled annual evolution of the port seabed show very good agreement, which confirms the reliability and robustness of the hydrodynamic and sediment transport model and demonstrates the potential importance of an integrated modeling approach in optimizing the management of port activities.

The assumption of unvarying initial bathymetry conditions in the different scenarios deserves some additional consideration, as it undoubtedly introduces some inaccuracy into the results. This approach does not consider the real order of vessels' passages or the impact that the evolving seabed has on the hydrodynamics and sediment transport simulations. In particular, the variable clearance distance between the propeller's tip and the seabed due to the evolving erosion/deposition processes is not considered, although this will increase the differences over time. However, the complexity of the system requires the introduction of several approximations, such as the dimension and rotation rates of the propellers, the typology and distribution of the sediment, the layering of the sea bed, the shear stress for erosion and deposition, or the constant initial bathymetry. A solution for the bathymetry issue could be to implement the system in operational mode, and thus continually updating the initial bottom boundary conditions through the simulation iterations. However, this was not realistic in terms of computational effort, and was beyond the scope of the study, which was to identify areas of erosion and deposition in the port and to evaluate the order of magnitude of the corresponding evolution rates to support the port management. Nevertheless, if we consider the most significant variation of the seabed and the typical propeller induced bottom velocities, which are in the order of 50 cm (Figure 12) and 1-2 ms^{-1} (Figures 7, 9 and 10), respectively, the resulting bottom shear stresses are in the order of 2-4 Nm^{-2}. Such values are orders of magnitude larger than the typical critical shear stress for the deposition-erosion of freshly deposited fine sediments (in the order of 0.07-0.15 Nm^{-2}, respectively), suggesting that variations in the bottom shear stresses due to a change in the clearance distance of the propeller's tip of an order of 50 cm (a conservative estimate), would not have a significant impact on the mobility of the sediments. Consequently, such differences would not imply substantial variations in the erosional and depositional processes and patterns.

5 – Summary and Conclusions

The impact of naval traffic on the seabed of the passenger port of Genoa was investigated through numerical modeling. The combination of a very high resolution, non-hydrostatic, circulation model (MIKE 3 HD FM) with a sediment transport model (MIKE 3 MT FM), based on unstructured grids on the horizontal and on sigma levels on the vertical, enabled us to reconstruct the annual evolution of the port seabed. The final results of the modeling, in terms of maps of erosion and deposition inside the basin, were qualitatively supported by observational evidence. Our approach was to simulate only one arrival and one departure from each dock of the port and to analyze the impact of a single naval passage on the seabed in terms of sediment concentration, motion and distribution.

From the traffic analysis in the port for a typical year (2017), we could obtain the detailed situation of the number of arrivals and departures for each dock as a starting point for the study. By superimposing the effects of single vessels weighted for the annual number of passages of the most representative vessel operating on each dock, an annual map of erosion/deposition was reconstructed and validated on a semi-quantitative basis by comparison with various bathymetric surveys for the same period.

In general, the simulations showed that the velocity intensities on the bottom induced by propeller-generated jets can reach almost 2 ms^{-1}, and mainly depend on the dimensions of the propellers, the rotation rate and the distance between the propeller and the bottom. Such velocities may reach up to 8-9 ms^{-1} at the propeller's axis depth, and penetrate horizontally through the water for long distances, up to at least 40-50 times the propeller's diameter. The bed shear stresses induced by these velocities, and the propeller jet induced entrainment, mobilize and re-suspend large amounts of the fine and less compacted sediments present inside the port. Fine proportions with lower fall velocities tend to remain in suspension for longer periods of time, resulting in the creation of sediment plumes.

Our findings showed how significant these deposition rates can be in a densely operated port, reaching values of several tens of centimeters per year in specific areas.

Our approach enabled us to minimize the computational time and also decompose the overall complex view of sediment transport of the entire port into several simpler views. Consequently, we were able to analyze the specific hydro and sediment dynamics for each dock and vessel, and to identify specific routes responsible for particularly serious erosion and accumulation, as historically reported by the managing authorities of the port operations and traffic. The range of current intensities induced by the propeller action was identified along the water column, and this can be further used as a sound and scientifically based benchmark value for potential defensive actions on the seabed and port structures, to guarantee the ongoing full operability of the port.

The most significant mechanisms for the port's hydro and sediment dynamics that occur during vessel passages were identified and the subsequent analysis identified how and why specific areas are subject to erosion and other areas are subject to deposition, and the extent of these mechanisms. In particular, the mechanism of ongoing erosion along the docks walls and of deposition along the central portions of the mooring basins were identified and explained, along with the ongoing deposition process in the area between the heads of *Ponte dei Mille* and *Molo Vecchio*. Identifying and reproducing this process for the port managers was particularly important as it occurs at a very significant rate of up to 40-50 cm per year in some areas. Finally, the natural hole located off the heads of *Ponte Colombo* and *Ponte Assereto* was identified through the model as an area of erosion, although at significant depth. This is mainly due to the turning maneuvers carried out by vessels in this area, and partially corresponds to one of the turning basins of the port and involves approximately 50% of its entire traffic (docks T5, T6 and T7). This location has historically been used as a dumping site for the material resulting from seabed maintenance dredging, but our study showed how unfit this area is for such purpose, as the freshly deposited sediment is soon re-suspended by the intense currents induced by the vessels turning operations.

The importance of this study is not only to confirm how an integrated high resolution modeling can reproduce the most significant and complex mechanisms of hydrodynamics and sediment transport occurring inside ports, which was successfully achieved, but it also suggests that it can be used as a tool for optimizing port management. It could be applied to regulating the naval traffic in ports and thus identifying the most suitable schedule and routing in terms of sediment concentrations, bottom velocities, erosion, accumulation and vessel drafts. It could also be used to identify the largest vessels that can potentially operate in the docks when planning future commercial traffic, or to study the impact of increased port traffic on the seabed and on the port's structures. Finally, in recurring dredging operations, most busy ports must regularly face sediment accumulation problems, and our tool can therefore inform awareness planning of such activities so the authorities are fully prepared.

Daily fully-operational implementations of similar integrated systems can also be set up, as the daily schedule of the port is known. This would enable the continuous monitoring of the evolution of the seabed and allow authorities to be constantly and fully aware of the potential criticalities they face.

Future research following on from this study should also consider the effect of the Bernoulli wake in combination with the propeller's induced jets on sediment resuspension, advection and dispersion. This mechanism was not considered in the present version of the system. The current intensities caused by vessels' generated waves during and after their passages will be smaller than those induced by propellers along their axes, but they tend to penetrate along the water column and reach the bottom, thus carrying a significant amount of energy, and possibly re-suspending a substantial amount of solid material (Rapaglia et al., 2011), which is likely to enhance vertical mixing and may induce the sediment to be suspended for longer periods and at higher depths.

APPENDIX A1 – Hydrodynamic model governing equations

MIKE 3 Flow Model FM is based on the Navier-Stokes equations for an incompressible fluid under the assumptions of Boussinesq. The governing equations of the model are the equations of momentum (A1.1) and mass continuity (A1.2), the equations of heat and salinity transport (A1.3 and A1.4, respectively) and the equation of state (A1.5) based on the UNESCO formula of 1981 (UNESCO, 1981a). Considering a Cartesian coordinate system *(x,y,z)* we have:

$$\frac{\partial u}{\partial x}+\frac{\partial v}{\partial y}+\frac{\partial w}{\partial z}=0 \qquad \text{(A1.1)}$$

$$\frac{\partial u}{\partial t}+\frac{\partial u^2}{\partial x}+\frac{\partial vu}{\partial y}+\frac{\partial wu}{\partial z}=fv-\frac{1}{\rho_0}\frac{\partial q}{\partial x}-g\frac{\partial \eta}{\partial x}-\frac{1}{\rho_0}\frac{\partial p_a}{\partial x}-\frac{g}{\rho_0}\int_z^{\eta}\frac{\partial \rho}{\partial x}dz+F_u+\frac{\partial}{\partial z}\left(\nu_t^v\frac{\partial u}{\partial z}\right) \qquad \text{(A1.2.1)}$$

$$\frac{\partial v}{\partial t}+\frac{\partial v^2}{\partial y}+\frac{\partial uv}{\partial x}+\frac{\partial wv}{\partial z}=fu-\frac{1}{\rho_0}\frac{\partial q}{\partial y}-g\frac{\partial \eta}{\partial y}-\frac{1}{\rho_0}\frac{\partial p_a}{\partial y}-\frac{g}{\rho_0}\int_z^{\eta}\frac{\partial \rho}{\partial y}dz+F_v+\frac{\partial}{\partial z}\left(\nu_t^v\frac{\partial v}{\partial z}\right) \qquad \text{(A1.2.2)}$$

$$\frac{\partial w}{\partial t}+\frac{\partial w^2}{\partial z}+\frac{\partial uw}{\partial x}+\frac{\partial wv}{\partial y}=-\frac{1}{\rho_0}\frac{\partial q}{\partial z}+F_w+\frac{\partial}{\partial z}\left(\nu_t^v\frac{\partial w}{\partial z}\right) \qquad \text{(A1.2.3)}$$

$$\frac{\partial T}{\partial t}+\frac{\partial uT}{\partial x}+\frac{\partial vT}{\partial y}+\frac{\partial wT}{\partial z}=F_T+\frac{\partial}{\partial z}\left(D_{ts}^v\frac{\partial T}{\partial z}\right)+\hat{H} \qquad \text{(A1.3)}$$

$$\frac{\partial S}{\partial t}+\frac{\partial uS}{\partial x}+\frac{\partial vS}{\partial y}+\frac{\partial wS}{\partial z}=F_s+\frac{\partial}{\partial z}\left(D_{ts}^v\frac{\partial S}{\partial z}\right) \qquad \text{(A1.4)}$$

$$\rho=\rho(S,T) \qquad \text{(A1.5)}$$

Since we used the barotropic density mode the only hydrodynamic equations used for the present work are A1.1 and A1.2. The symbols used in the governing equations of the model are presented in Table 4

Table 4 – Symbols used in the governing equations A1

x,y,z	Cartesian coordinate system
u,v,w	components of the field of velocity [ms^{-1}]
g	gravity acceleration [ms^{-2}]
ρ	water density [kgm^{-3}]
ρ_0	reference value for water density [kgm^{-3}]
q	non-hydrostatic pressure [Pa]
p_a	atmospheric pressure at the sea surface [Pa]
f	Coriolis parameter (non-dimensional)

ν_t^v	vertical eddy viscosity [m^2s^{-1}]
F_u, F_v, F_w	horizontal diffusivity
T	temperature [°C]
S	Salinity [PSU]
F_T, F_S	Horizontal diffusion terms for T and S
D_{ts}^v	vertical eddy diffusivity [m^2s^{-1}]
$\hat{H}$	Source term due to heat exchange with the atmosphere

APPENDIX A2 – Mud transport model governing equations and parameterizations

The sediment transport module is based on the advection dispersion equation for a passive tracer in an incompressible fluid. The tracer is the concentration *C* of sediment along the water column. The field velocity used for advection is the one calculated through the hydrodynamic set of equations of Appendix A1. The symbols used in the set of equations A2 are summarized in Table 5

$$\frac{\partial C}{\partial t} + \frac{\partial}{\partial x}(uC) + + \frac{\partial}{\partial y}(vC) + \frac{\partial}{\partial z}[(w + w_s)C] = \frac{\partial}{\partial z}\left(D_C^v \frac{\partial C}{\partial z}\right) + F_C \quad \text{(A2.1)}$$

The vertical bottom boundary condition for sediment flux is expressed as:

$$D_C^v \frac{\partial C}{\partial z}\bigg|_{z=-H} - w_s C = S \quad \text{(A2.2)}$$

and the sediment flux *S* at the bottom is calculated through the approach of Krone (1962) for deposition (Eq. A2.3), through that of Partheniades (1965) for erosion of consolidated sediment (Eq. A2.4) and through that of Parchure and Metha (1985) for erosion of soft or unconsolidated sediment (Eq. A2.5).

$$S_d = w_s c_b p_d \quad \text{(A2.3)}$$

where

$$p_d = 1 - \frac{\tau_b}{\tau_{cd}} \qquad \text{valid for } \tau_b < \tau_{cd} \quad \text{(A2.3.1)}$$

$$S_{ec} = E\left(\frac{\tau_b}{\tau_{ce}} - 1\right)^n \qquad \text{valid for } \tau_b \geq \tau_{ce} \text{ and hard bed} \quad \text{(A2.4)}$$

$$S_{es} = E\ exp\left[\alpha(\tau_b - \tau_{ce})^{1/2}\right] \qquad \text{valid for } \tau_b \geq \tau_{ce} \text{ and soft bed} \quad \text{(A2.5)}$$

The settling velocity for sediment is calculated through the Stokes law (A2.6).

$$w_s = \frac{gd^2}{18}\left(\frac{\rho_s}{\rho_w} - 1\right) \quad \text{(A2.6)}$$

Table 5 – symbols used in the equations and parameterizations A2 of the sediment transport model

x,y,z	Cartesian coordinate system (same as Table 4)
u,v,w	components of the field of velocity (same as Table 4) [ms^{-1}]
C	sediment concentration [gmc^{-1}]
C_b	sediment concentration in the bottom layer [gmc^{-1}]
w_s	settling velocity [ms^{-1}]
D_C^v	vertical eddy diffusivity for C (same as for T and S) [m^2s^{-1}]
F_C	horizontal diffusion terms for C
H	water depth [m]
S_e	bottom sediment flux for erosion [kgm^2s^{-1}]
S_d	bottom sediment flux for deposition [kgm^2s^{-1}]
$S_{e,s}$	bottom sediment flux for erosion of soft bed [kgm^2s^{-1}]
$S_{e,c}$	bottom sediment flux for erosion of consolidated bed [kgm^2s^{-1}]
p_d	probability of deposition for the sediment [non dimensional]
τ_b	bottom shear stress [Nm^{-2}]
τ_{bd}	critical stress for deposition [Nm^{-2}]
τ_{ce}	critical stress for erosion [Nm^{-2}]
E	bottom erodibility [Nm^{-2}]
α	empirical coefficient [$m/\sqrt{N}$]
n	Power of erosion (empirical non-dimensional)
d	diameter of grains [m]
ρ_s	density of dried sediment [kgm^{-3}]
ρ_w	density of water[kgm^{-3}]
g	gravity acceleration [ms^{-2}]

APPENDIX A3 – Results of total bed change

The following matrix of plots presents the results in terms of sediment erosion and accumulation for a single undocking (left) and docking (right) respectively for the scenarios of docks T1, T2, T3, T5, T6, T9, T10, T11, DL, 1003, (top to bottom).

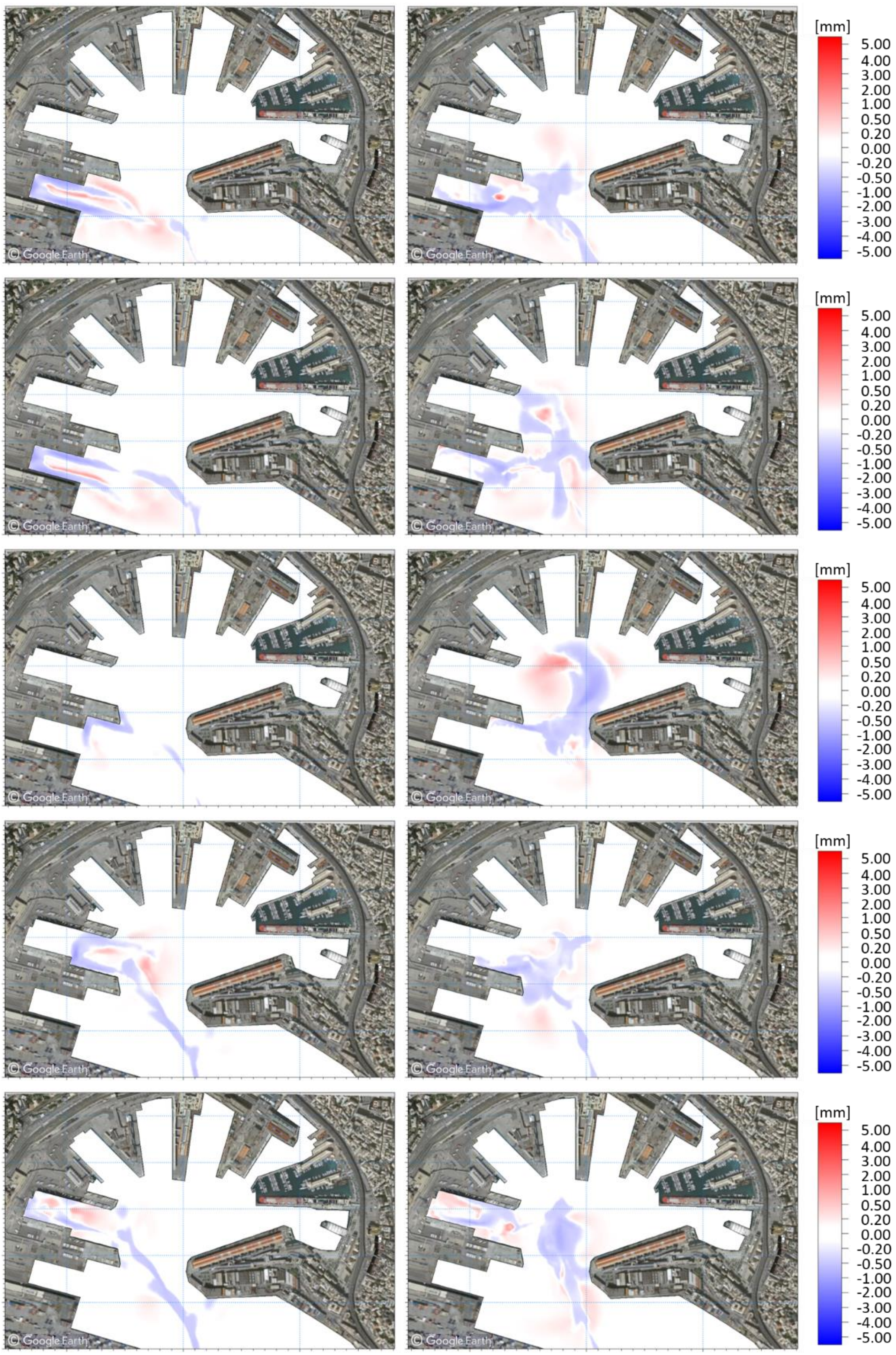
[mm]
5.00
4.00
3.00
2.00
1.00
0.50
0.20
0.00
-0.20
-0.50
-1.00
-2.00
-3.00
-4.00
-5.00
© Google Earth

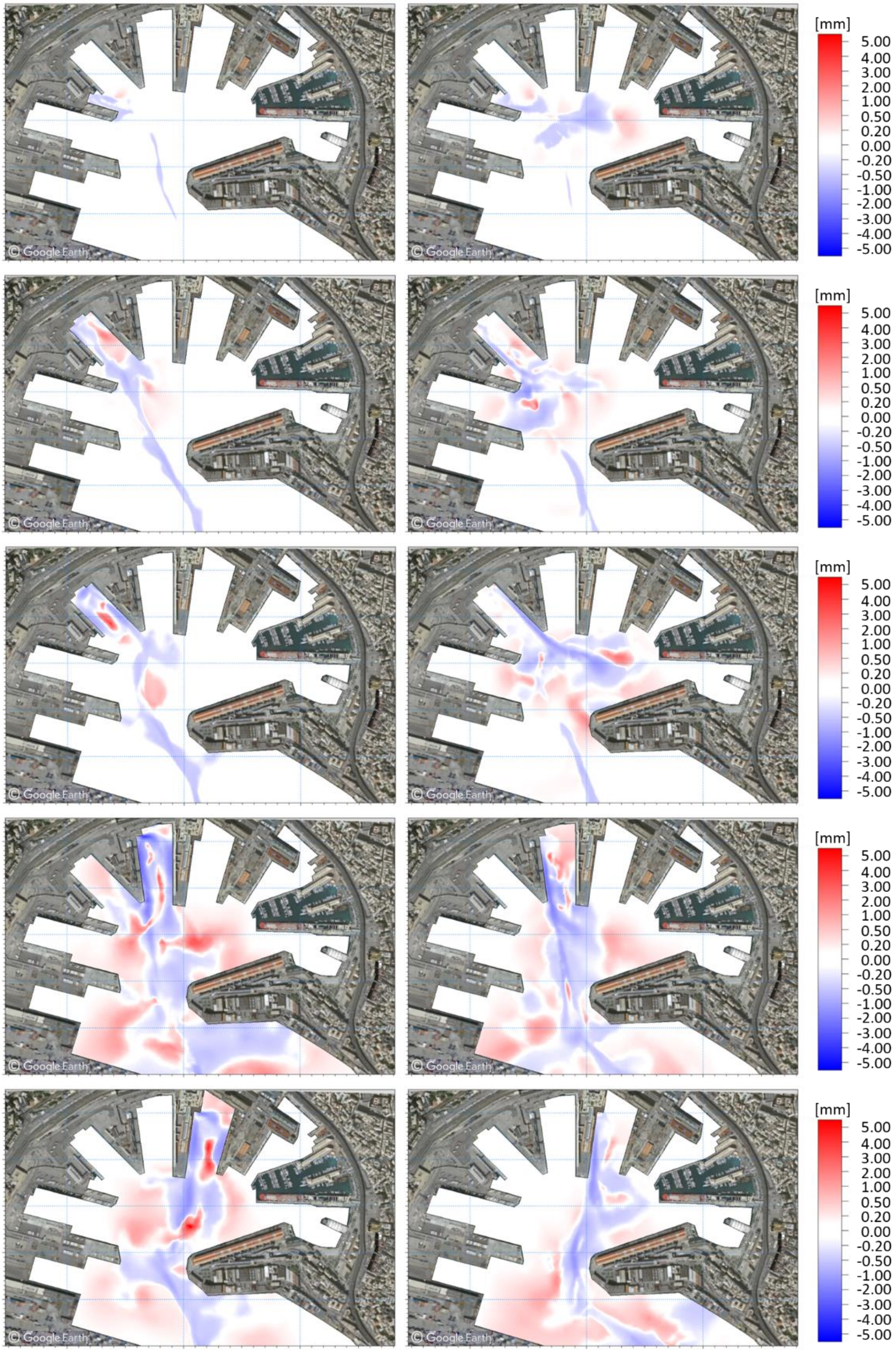
[mm]
5.00
4.00
3.00
2.00
1.00
0.50
0.20
0.00
-0.20
-0.50
-1.00
-2.00
-3.00
-4.00
-5.00
© Google Earth

Data Availability

The modelling dataset including the simulations produced for the present study covers a volume wider than 2 TB. Such an amount of data raises an evident problem in order to make them available on data repositories. Consequently, the output of the simulations won't be directly available. However, the model set-up and all the files necessary for their reproduction will be made available in MIKE FM format upon request to the corresponding author.

Team list

Antonio Guarnieri (first and corresponding author), Sina Saremi (co-author), Andrea Pedroncini (co-author), Jakob H. Jensen (co-author), Silvia Torretta (co-author), Caterina Vincenzi (co-author), Marco Vaccari (co-author).

Author contributions:

Antonio Guarnieri implemented the numerical models and simulations, post-processed the raw output, analysed the results and wrote the manuscript;

Sina Saremi gave technical and scientific support during the implementation of the models, provided the code for the propellers modelization as input to MIKE and supported the writing and finalization of the manuscript;

Andrea Pedroncini first conceived the idea of the methodology adopted in the study, gave scientific support for the implementation of the models and feedback during the writing of the manuscript;

Jacob H. Jensen provided scientific support and advice regarding the driving mechanisms of naval induced sediment dynamics;

Silvia Torretta provided technical support for the model implementation and for the observed bathymetry analysis and reconstruction;

Caterina Vincenzi and Marco Vaccari provided bathymetry data, sediment data and information on dredging activities and general sediment related issues. They also favored the acquisition of the naval traffic data.

Competing interests:

Caterina Vincenzi and Marco Vaccari are employees of the Port Authority of Genova (Autorità di Sistema Portuale del Mar Ligure Occidentale), which commissioned and funded the present study to DHI, a private not-for-profit consultancy and research company in the field of water. Andrea Pedroncini, Silvia Torretta, Sina Saremi and Jakob H. Jensen are DHI employees. Antonio Guarnieri was DHI employee when the study was conducted; he is now employed at Istituto Nazionale di Geofisica e Vulcanologua (INGV).

Acknowledgments

We are grateful to Stazioni Marittime SpA for providing the daily traffic data of the Port of Genoa which was the starting point for this study. We are particularly grateful to Captain Calcagno of Stazioni Marittime SpA for the qualified and experienced information he gave on the sediment and vessels' dynamics in the port, which helped set up the numerical models, interpret and rely on the final results.

We are also particularly grateful to both the anonymous referees who revised the first version of the manuscript since their constructive critique and comments helped us enrich and improve the final version of the article.

References

- Abromeit, U., Alberts, D., Fischer, U., Fleischer, P., Fuehrer, M., Heibaum, M., Kayser, J., Knappe, G., Köhler, H.J., Liebrecht, A., Reiner, W., Schmidt-vöcks, D., schulz, H., Schuppener, B., Söhngen, B., Soyeaux, R.: Principles for the Design of Bank and Bottom Protection for Inland Waterways, 1st Edition, Bundesanstalt für Wasserbau, Karlsruhe, 2010.
- Amorim, J.C.C., Bundgaard, K. and Elfrink, B.,: Environmental impact assessment of dredging deep in the navigation channel of the Port of Santos. In Environmental Hydraulics, Two Volume Set (pp. 639-644). CRC Press, 2010
- Castells-Sanabra, M., Mujal-Colilles, A., LLull, T., Moncunill, J., Martínez de Osés, F., & Gironella, X.: Alternative Manoeuvres to Reduce Ship Scour. Journal of Navigation, 1-18. doi:10.1017/S0373463320000399, 2020
- Ciccacci, S., D'Alessandro, L., Fredi, P., and Lupia Palmieri, E. (1989). Contributo dell'analisi geomorfica quantitativa allo studio dei processi di denudazione nel bacino idrografico del Torrente Paglia (Toscana meridionale - Lazio settentrionale),Suppl. Geogr. Phys. Dinam. Quat., I, 171-188, https://doi.org/10.13140/2.1.2991.6802, 1989.
- CIRIA, CUR, CETMEF: The Rock Manual. The use of rock in hydraulic engineering, 2nd edition, C683 CIRIA, London, 2007.
- DHI: MIKE 3 Flow Model HD FM - Hydrodynamics Flexible Mesh - Scientific Documentation, DHI, Hørsholm, 2017.
- DHI: MIKE 3 MT FM - Mud Transport Flexible Mesh - Scientific Documentation, DHI, Hørsholm, 2019.
- Flather, R.: A tidal model of the northwest European continental shelf, Memories de la Societe Royale des Sciences de Liege, 6, 10, 141–164, 1976.

- Grabe, J., Van Audgaerden, T., Busjaeger, D., Gerrit de Gijt, J., Heibaum, M., Heimann, S., Van der Horst, A., Kalle, H.U, Krengel, R., Lamberts, K.H., Miller, C., Morgen, K., Peshken, G., Retzlaff, T., Reuter, E., Richwein, W., Ruland, P., Schrobenhausen, W. S., Tworushka, H., Vollstedt, H.W.: Recommendations of the Committee for Waterfront Structures, Harbours and Waterways - EAU 2012, 9^{th} Edition, Issued by the Committee of Waterfront Structures of the German Port Technology Association and the German Geotechnical Society, Ernst & Sohn GmbH & Co., Berlin, 661, 2015.
- Grant W. and Madsen O.: Combined wave and current interaction with a rough bottom, J. Geophys. Res., 84, 1797–1808, 1979.
- Hamill, G.A.: Characteristics of the screw wash of a maneuvering ship and the resulting bed scour, Ph.D. dissertation, Queen’s Univ. of Belfast, Belfast, Northern Ireland, 1987.
- Hamill, G. A., Johnston, H. T., Stewart, D. P.: Propeller Wash Scour near Quay Walls, Journal of Waterway, Port, Coastal, and Ocean Engineering, 170-175,V 125, 4, https://doi.org/10.1061/(ASCE)0733-950X(1999)125:4(170), 1999
- Kristensen, H. O.: Analysis of technical data of Ro-Ro ships, in: Report n. 02 - of Project n. 2014-122 Mitigating and reversing the side-effects of environmental legislation on Ro-Ro shipping in Northern Europe, HOK Marineconsult ApS, 2016.
- Krone, R.: Flume studies of the transport of sediment in estuarial processes: Final Report, Hydraulic Engineering Laboratory and Sanitary Engineering Research Laboratory, Univ. of California, Berkely, 1962.
- Lam, W.H., Hamill, G., Robinson, D., Raghunathan, R., and Kee, C., Submerged propeller jet, WSEAS Conferences, Udine, Italy, 20-22 January 2005.
- Leonard, B.P.: The ULTIMATE conservative difference scheme applied to unsteady one-dimensional advection, Comput. Method Appl. M., 88, 17-74, https://doi.org/10.1016/0045-7825(91)90232-U, 1991.
- Lisi, I., Feola, A. , Bruschi, A., Di Risio, M., Pedroncini, A., Pasquali, D., and Romano, E.,: La modellistica matematica nella valutazione degli aspetti fisici legati alla movimentazione dei sedimenti in aree marino-costiere, Manuali e Linee Guida ISPRA, 169/2017, 144., 2017.
- MarCom Working Group 180: PIANC REPORT N° 180 - Guidelines for Protecting Berthing Structures from Scour Caused by Ships, PIANC Secrétariat Général., Bruxelles, 2015.
- Mujal-Colilles, A., Gironella, X., Sanchez-Arcilla, A., Puig Polo, C., and Garcia-Leon, M.: Erosion caused by propeller jets in a low energy harbour basin, J. Hydraul. Eng., https://doi.org/10.1080/00221686.2016.1252801, 2016.

- Mujal-Colilles, A., Castells, M., Llull, T., Gironella, X., Martínez de Osés, X.: Stern Twin-Propeller Effects on Harbor Infrastructures. Experimental Analysis. Water 2018, 10, 1571.
- Parchure, T., and Metha, A.: Erosion of soft cohesive sediment deposits, J. of Hydraul. Eng., 111, 10, 1308-1326, https://doi.org/10.1061/(ASCE)0733-9429(1985)111:10(1308), 1985.
- Partheniades, E.: Erosion and deposition of cohesive soils, Journal of the Hydraulics Division, 91, 105-139, 1965.
- Rapaglia, J., Zaggia, L., Ricklefs, K. , Gelinas M., and Bokuniewicz, H.: Characteristics of ships' depression waves and associated sediment resuspension in Venice Lagoon, Italy: J. Marine Syst., 85, 45-56, https://doi.org/10.1016/j.jmarsys.2010.11.005, 2011.
- Sanford, L.P. and Maa, J.P.Y.: A unified erosion formulation for fine sediments. Marine Geology, 179 (1-2), pp.9-23, 2001
- Soulsby, R., Hamm, L. , Klopman, G., Myrhaug, D., Simons, R., and Thomas, G.: Wave-current interaction within and outside the bottom boundary layer, Coast. Eng., 21, 41-69, 1993.
- Teeter, A.: Vertical transport in fine-grained suspension and nearly-deposited sediment, in: Estuarine Cohesive Sediment Dynamics, 14, Mehta, A.J., Springer Verlag, 126-149, https://doi.org/DOI:10.1029/LN014, 1986.
- Teisson, C., Ockenden, M., Le Hir, P., Kranenburg, C. and Hamm, L.,: Cohesive sediment transport processes. Coastal Engineering, 21(1-3), pp.129-162, 1993
- UNESCO, The practical salinity scale 1978 and the international equation of state of sea water, UNESCO Technical Papers in Marine Science 36, 25 pp.,1981a."
- Van Rijn, L.: Unified view of sediment transport by currents and waves. Initiation of motion, bed roughness, and bed-load transport, J. Hydraul. Eng., 133, 6, 2007.
- Verhei, H. J.: The stability of bottom and banks subjected to the velocities in the propeller jet behind ships, 8th International Harbour Congress, Antwerp, June 13-17, 303, 1983.
- Winterwerp, J., and Van Kesteren, W.: Introduction to the Physics of Cohesive Sediment in the Marine Environment, 1st Edition, 56, Elsevier B.V., Amsterdam, 576, 2004.
- Yuksel, Y., Tan, Y., Celikoglu, Y.: Determining propeller scour near a quay wall. Oc. Eng., 188, 2019.